

Exploration of a Class of Aryl Imidazolyl Ureas As Potent Acid Ceramidase Inhibitors for the Treatment of Fibrotic Diseases

Richard Beresis, Vijaya Prathigudupu, Carson Cable, Amy Yu, Marc Adler, Roopa Ramamoorthi, Seul Ki Yeon, John D. Gordan, Sachin Sharma, William F. DeGrado, Balyn Zaro, Jennifer Y. Chen, and Hyunil Jo*



Cite This: *ACS Omega* 2025, 10, 34747–34761



Read Online

ACCESS |



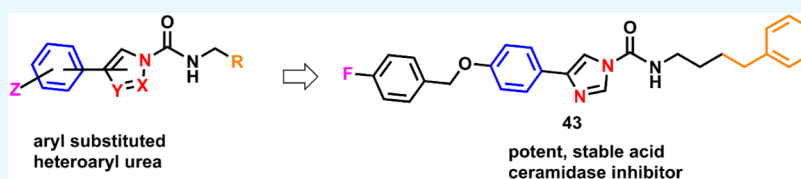
Metrics & More



Article Recommendations



Supporting Information



ABSTRACT: Acid ceramidase (aCDase) is an essential enzyme in sphingolipid metabolism and has been linked to various pathological conditions, including cancer and fibrosis. In our previous studies, we observed that inhibiting aCDase with B13 (4) helped alleviate liver fibrosis in mouse models and in ex vivo human precision-cut liver slices. However, B13 (4) showed limited potency, prompting us to search for more effective aCDase inhibitors. During our exploration of well-established urea-type inhibitors, we discovered that the aryl imidazolyl urea scaffold demonstrated both high potency and chemical stability. Among the tested compounds, compound 43 stood out with its nanomolar IC_{50} activity against aCDase and its ability to significantly reduce fibrosis markers, such as collagen production, in hepatic stellate cells. Kinetic studies were also performed to understand the interaction of compound 43 with aCDase. Additionally, proteomics analysis of activated hepatic stellate cells treated with compound 43 revealed a notable change in several cellular proteins, including those related to growth factors, such as platelet-derived growth factor receptor (PDGFR). These results indicate that the aryl imidazolyl urea scaffold holds strong potential for further development as a therapeutic option for fibrotic diseases.

INTRODUCTION

Liver fibrosis is a condition characterized by the excessive accumulation of extracellular matrix (ECM) components, particularly collagen, which leads to tissue stiffening, structural disruption, and impaired organ function.^{1–4} This condition can result from various etiologies, including alcohol use, viral infections (such as chronic hepatitis B virus or hepatitis C virus), and metabolic dysfunction-associated liver disease (MASLD).⁵ Treatment options for liver fibrosis have historically been limited. However, recent advances in targeting lipid metabolism have opened new avenues for therapy, including the FDA approval of Resmetirom in 2024, a thyroid hormone receptor beta (THR- β) agonist, as the first drug for MASH (metabolic dysfunction-associated steatohepatitis) with liver fibrosis. While Resmetirom shows promising effects on disease pathophysiology, its efficacy in promoting fibrosis regression remains modest.⁶ Thus, there is an urgent need to identify new approaches to reverse fibrosis in patients with established disease.

The role of lipid metabolism in liver fibrosis has been further highlighted by our recent research.^{7,8} In our work, we focused on acid ceramidase (aCDase), a lysosomal enzyme crucial for breaking down ceramide into fatty acids and sphingosine (Figure 1A). We found that inhibiting aCDase pharmacolog-

ically using B13 (4) improves liver fibrosis, suggesting its potential to reverse the condition (Figure 1B). However, B13 (4) lacked the potency necessary for further development,⁸ prompting us to search for more potent aCDase inhibitors.

Since its discovery as an amide hydrolase in rat brains in 1963,⁹ aCDase has been the focus of extensive research, leading to the development of various inhibitors (Figure 1B). This enzyme is initially produced as a single 53–55 kDa precursor polypeptide, which undergoes post-transcriptional modifications and autocleavage in lysosomes to form a heterodimer consisting of α (13 kDa) and β (40 kDa) subunits.¹⁰ In 2018, the crystal structure of aCDase was determined in both its pro-form and active form, revealing that activation creates a hydrophobic channel leading to the active site cysteine residue (Cys 143).^{11–13} Additionally, the crystal structure of aCDase bound to the covalent inhibitor carmofur

Received: April 23, 2025

Revised: July 14, 2025

Accepted: July 23, 2025

Published: July 31, 2025



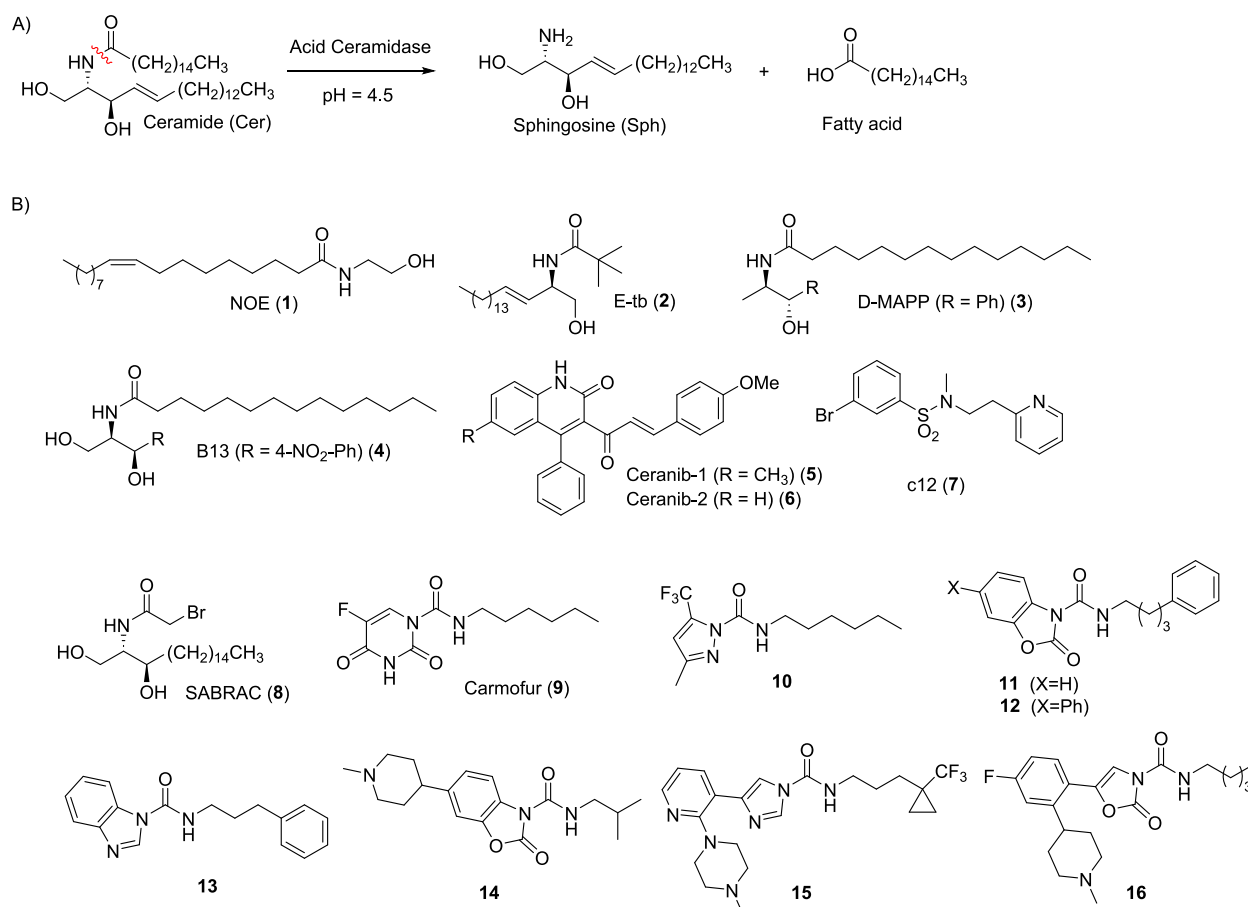


Figure 1. Function of aCDase and its representative inhibitors. A) hydrolysis of ceramide by aCDase. ACDase hydrolyzes ceramide into sphingosine and fatty acid. B) Representative examples of known aCDase inhibitors.

(9) has been reported, providing valuable insights into the mechanism of covalent inhibition.^{14,15}

aCDase functions optimally at a pH of 4.5, catalyzing the hydrolysis of ceramides into sphingosine and fatty acids, with a preference for unsaturated ceramides containing 6 to 16-carbon acyl chains.¹² Interestingly, like many enzymes, aCDase can also catalyze the reverse reaction, synthesizing ceramide from sphingosine and a fatty acid (C12) at an optimal pH of 6.¹³ aCDase plays a crucial role in maintaining the balance between ceramide and sphingosine levels in lysosomes, particularly through the salvage pathway.¹⁶

Ceramide is well-known for its association with cell growth arrest and apoptosis, whereas sphingosine-1-phosphate (S1P), derived from sphingosine, promotes cell survival and proliferation.^{17,18} This balance between ceramide and S1P, often referred to as the sphingolipid rheostat, is essential for determining cell fate.¹⁹ Notably, aCDase has been found to be upregulated in various neurodegenerative diseases and cancers, including Alzheimer's disease, prostate cancer, acute myeloid leukemia (AML), and melanoma.^{20–23} Consequently, aCDase has emerged as a significant therapeutic target, and several inhibitors have already been identified, providing valuable direction for future inhibitor design (Figure 1B).

N-Oleylethanolamine (NOE, 1) was the first ceramide-mimicking aCDase inhibitor reported in the literature, but it showed very low potency ($K_i = 700 \mu\text{M}$).²⁴ Later, an improved NOE analogue, E-tb (2), was identified by Bedia et al., demonstrating significantly enhanced potency ($\text{IC}_{50} = 13.5$

μM) in intact cell assays.²⁵ Meanwhile, Bielawska et al. explored *N*-acylphenylaminoalcohol analogues such as D-MAPP (3) and B13 (4) as ceramidase inhibitors.²⁶ D-MAPP exhibited low potency against aCDase ($\text{IC}_{50} > 500 \mu\text{M}$) in HL-60 lysate assays but showed better activity against alkaline ceramidase ($\text{IC}_{50} = 1\text{--}5 \mu\text{M}$). In contrast, B13 (4), which differs from D-MAPP in stereochemistry and includes a nitro (NO_2) functional group, was more water-soluble and more effective in inhibiting aCDase ($\text{IC}_{50} = 10 \mu\text{M}$).²⁷

In a search for small molecule aCDase inhibitors lacking long alkyl chains, Draper et al. discovered a novel inhibitor, ceranib-1 (5), through the screening of a commercial library of 50,000 compounds using SKOV3 cells. An analogue synthesized chemically, ceranib-2 (6), exhibited slightly better potency ($\text{IC}_{50} = 20\text{--}30 \mu\text{M}$) compared to ceranib-1 ($\text{IC}_{50} = 50\text{--}60 \mu\text{M}$) in SKOV3 cell assays.²⁸ More recently, a high-throughput screening of 4,000 compounds using melanoma cell lysate identified several promising inhibitors, with the most potent, c12 (7), demonstrating similar efficacy in cell-based assays ($\text{IC}_{50} = 32 \mu\text{M}$).²⁹

While many noncovalent inhibitors displayed modest to poor potency, a breakthrough came in 2013 by two research groups. The Fabrias lab introduced SABRAC (8), a potent aCDase inhibitor ($\text{IC}_{50} = 52 \text{ nM}$ in FX10 cell lysate assays).³⁰ SABRAC (8), derived from ceramide analogues modified with thiol-reactive groups (α -bromo acetamide), also served as an activity-based probe for aCDase and showed potential against oligodendroglioma.^{31,32} However, its ability to cross the

blood–brain barrier raised concerns about potential central nervous system side effects, particularly for liver fibrosis treatment.

The Piomelli lab also reported a powerful aCDase inhibitor, carmofur (9), with an IC_{50} of 52 nM.³³ Originally developed as a prodrug of 5-fluorouracil (5-FU), carmofur's release of 5-FU raised risks such as leukoencephalopathy,³⁴ highlighting the need for further medicinal chemistry efforts to replace the leaving group. Subsequent research led to new compounds where 5-FU was replaced by heterocycles, including pyrazole (10),³⁵ benzoxazolone (11–12, 14)^{36–38} and benzimidazole (13).³⁹ While these compounds showed excellent potency, their stability under various conditions (pH, plasma, metabolic) often required further optimization for development.

Extensive medicinal chemistry efforts by Scarpelli's group focused on the benzoxazolone scaffold, leading to the identification of an orally available compound, 14 (IC_{50} = 166 nM), where piperidine substitution improved solubility.³⁶ At the start of our project, little was known about alternative scaffolds that could offer a balance of potency and stability. Guided by Piomelli's earlier findings,^{37,38} we concentrated on aryl-substituted heterocycles. Notably, substituting a phenyl ring on the benzoxazolonyl urea scaffold, as seen in compound 12, significantly enhanced buffer stability compared to the unsubstituted compound 11. During our exploration, independently reported studies on aryl-substituted five-membered heterocycles (15, 16) further validated our approach, showcasing their potential as potent aCDase inhibitors.^{40,41} In this work, we present our research on phenyl-substituted imidazolyl urea as an alternative scaffold for acid ceramidase, offering a promising balance of potency and stability.

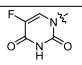
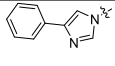
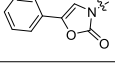
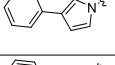
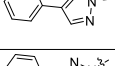
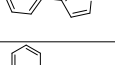
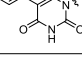
RESULTS

Our goal was to find new covalent inhibitors that target the active site cysteine (Cys 143) of aCDase. We initially screened over 50 compounds with various warhead groups, including ketoamides, α,β -unsaturated carbonyls, vinyl sulfones, and haloacetamides, but none exhibited sufficient potency (data not shown). Consequently, we refocused on the urea scaffold, aiming to improve its chemical and metabolic stability. Additionally, fine-tuning of reactivity can be readily achieved by modifying the aryl ring,³⁷ leading us to explore aryl-substituted heterocyclic urea as a potential new scaffold (Table 1). To ensure that any differences in potency were due solely to the phenyl-substituted heterocycles, we kept the alkyl chain on the right side of the urea moiety identical to that in carmofur (9). Syntheses of compounds followed the routine isocyanate chemistry for urea synthesis as described in the literature (Scheme 1).

Potency of synthesized compounds was measured using a fluorescence-based assay⁴² using the purified aCDase with a fluorescence substrate RBM14–12, following a protocol from the literature optimized for a 96-well format.⁴³ To preserve glycosylation, recombinant human aCDase (22–395, I93V) was expressed in High Five insect cells infected with baculovirus, following established protocols.¹¹ As a positive control, carmofur demonstrated a pIC_{50} of 7.62 in our assay, which was consistent with the reported value of 7.54.

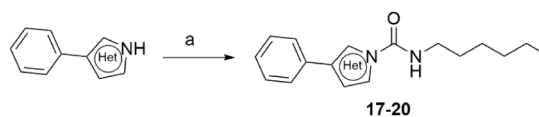
Our initial screening identified the phenyl-substituted imidazolyl urea (17) as particularly promising, displaying superior potency with a pIC_{50} of 8.03 (Table 1). In contrast, the phenyl-substituted oxazolone (18) displayed greater

Table 1. Exploration of Phenyl Substituted Heteroaryl Urea

ID	Heteroaryl	Potency ^a	Chemical stability ^b (% rem _{120min})	
			pH=4.5	pH=7.4
Carmofur (9)		7.6 ± 0.03	99%	99%
17		8.03 ± 0.09	67%	79%
18		6.67 ± 0.08	91%	99%
19		6.00 ± 0.17	Not tested	Not tested
20		5.96 ± 0.13	Not tested	Not tested
21		6.12 ^c	Not tested	Not tested
22		6.75 ^d	100% ^e	Not tested

^aPotency was expressed as $pIC_{50} \pm SEM$. ^bCompound remaining after incubation (120 min) at the specified pH. ^cFrom ref 35. ^dFrom ref 44. ^eFrom ref 44, % compound remaining after incubation (30 min).

Scheme 1. Synthetic Routes to Heteroaryl Urea Compounds^a



^aReagents and conditions: (a) *n*-hexyl isocyanate, DMAP, pyridine.

stability at both pH 7.4 and 4.5, representing plasma and lysosomal pH, respectively. However, urea scaffolds based on pyrrole (19) and pyrazole (20, 21) showed reduced potency. The phenyl-substituted uracil-derived urea (22) was also less active compared to carmofur (9) in terms of potency. Additionally, compound 17 demonstrated reasonable stability at both pH 7.4 and 4.5, with 79% and 67% remaining after 120 min of incubation, respectively, supporting its potential as a promising candidate for further investigation. Interestingly, the structurally related imidazolyl urea analogue (15), synthesized as reported in the literature,⁴¹ showed potent activity (pIC_{50} = 7.8) but only moderate chemical stability, with 23% remaining after 120 min of incubation at pH 7.4 (0% remaining at pH 4.5).

Encouraged by the excellent potency of the aryl-substituted imidazolyl urea 17, we investigated whether different substituents on the phenyl ring could further influence potency. In addition to pH stability, we also assessed their degradation in the presence of a high concentration of glutathione (5 mM) to identify compounds that can resist nonselective thiol attack, simulating a cellular environment.

We observed that most of the substituted phenyl imidazolyl urea compounds exhibited both good potency and stability in buffer and in the presence of glutathione (GSH). For example, the meta-methoxy substituted compound (23) showed

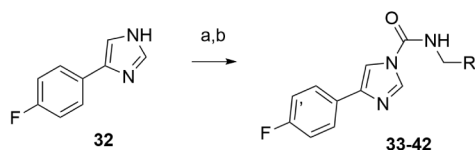
excellent potency ($\text{pIC}_{50} = 8.3$), although its stability was slightly compromised.

Interestingly, the position of the substituent (*ortho*, *meta*, *para*) did not significantly affect potency. For instance, the *meta*-OCH₃ (23) and *para*-OCH₃ (25) derivatives demonstrated similar potency. It is also noteworthy that *para*-F (24), *para*-CH₃ (28), and *para*-OBn (30) substitutions led to considerably enhanced stability in buffer (pH = 7.4) while maintaining strong potency.

Additionally, the electronic effects of the substituents did not substantially influence potency, as indicated by the comparable performance of *ortho*-Cl (26) and *ortho*-OH (27) derivatives. However, we recognized potential concerns regarding metabolic stability due to benzylic oxidation in compound 30.

Therefore, we selected the *para*-F substituted compound (24) for further investigation, given the straightforward synthesis for the readily availability of the starting materials. Accordingly, right-wing analogues (33–42) were readily synthesized using *p*-nitrophenylchloroformate chemistry to couple 4-fluorophenyl-1*H*-imidazole (32) with a range of amines (Scheme 2).

Scheme 2. Synthetic Routes to Right Wing Amine Analogues^a



^aReagents and conditions: (a) *p*-nitrophenylchloroformate, TEA, DCM, 0 °C (b) R-NH₂, TEA, DCM.

We tested various alkyl groups to explore alternatives to the *n*-hexyl alkyl chain in 24 (Table 3). While phenyl-substituted derivatives (33, 34, 35, 36) generally maintained acceptable potency, their stability decreased. Similarly, branched alkyl chains (38, 39) and cyclopropyl (37) and cyclobutyl groups (40, 41) did not enhance potency. Notably, the stereochemistry at the branched position affected potency (e.g., 38 vs 39), suggesting that the conformation and steric requirements of the alkyl chain are important. Neopentyl group (42) did not improve potency.

We observed that replacing the terminal CH₃ group with a phenyl group in compound 33 resulted in excellent potency, which can be attributed to hydrophobic interactions and

potential π - π interactions within the binding site. This explanation is further supported by molecular docking studies of compound 33 as a tetrahedral intermediate in aCDase, as suggested by previous research^{40,45} (Figure 2).

While no single compound demonstrated better potency and stability than 33, its stability under acidic conditions (pH 4.5) and in the GSH competition assay needed improvement. Previously, we found that introducing a benzyl ether substitution on the left wing (30, Table 2) conferred high

Table 2. Potency and Stability of Substituted Phenyl Imidazolyl Urea Series

ID	X	Potency (pIC_{50}) ^a	Stability ^b		
			pH=4.5	pH=7.4	5 mM GSH
17	<i>p</i> -H	8.0 ± 0.09	67%	79%	60%
23	<i>m</i> -OCH ₃	8.3 ± 0.02	42%	64%	43%
24	<i>p</i> -F	8.0 ± 0.05	55%	99%	66%
25	<i>p</i> -OCH ₃	8.0 ± 0.06	60%	74%	54%
26	<i>o</i> -Cl	7.9 ± 0.06	38%	64%	38%
27	<i>p</i> -OH	7.9 ± 0.06	55%	62%	41%
28	<i>p</i> -CH ₃	7.9 ± 0.06	88%	99%	83%
29	<i>o</i> -OH	7.9 ± 0.04	50%	86%	39%
30	<i>p</i> -OBn	7.9 ± 0.04	98%	100%	98%
31	<i>m</i> -Cl	7.6 ± 0.06	71%	84%	82%

^aPotency was expressed as $\text{pIC}_{50}(\text{M}) \pm \text{SEM}$. ^bStability was expressed by % compound remaining after incubation (120 min).

stability under acidic conditions as well as in the GSH competition assay. On the right wing, the addition of a terminal phenyl group (33, Table 3) not only increased potency but also improved stability in the same assay. To further enhance metabolic stability, a *para*-fluorine substitution was introduced on the benzyl ether moiety of 30 as a strategic medicinal chemistry modification, leading to the design of compound 43 (Scheme 3). The synthesis of 43 began with the O-alkylation of 4'-hydroxyacetophenone 44 using 4-fluorobenzyl chloride. This was followed by α -bromination with NBS

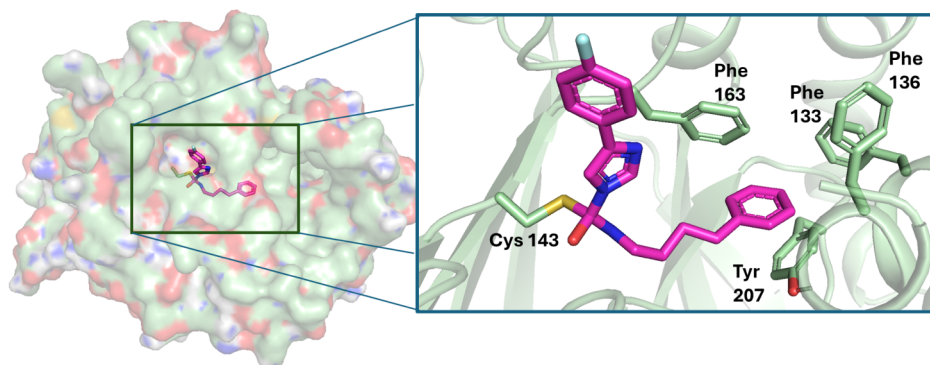
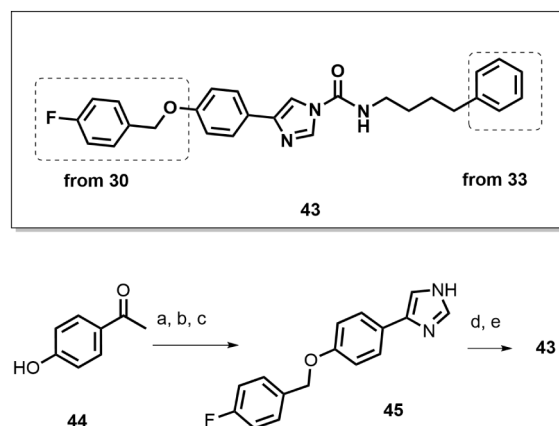


Figure 2. Tetrahedral intermediate model of 33 based on the X-ray structure of aCDase (PDB ID: 6MHM). The catalytic residue (Cys 143) and aromatic residues in the alkyl chain binding site are labeled.

Table 3. Exploration of Alkyl Chains

ID	Structure	Potency (pIC ₅₀) ^a	Stability ^b		
			pH=4.5	pH=7.4	5 mM GSH
24		8.0 ± 0.05	55%	99%	66%
33		8.5 ± 0.09	46%	64%	89%
34		8.2 ± 0.07	22%	47%	52%
35		7.9 ± 0.06	48%	63%	71%
36		7.9 ± 0.04	38%	54%	37%
37		7.6 ± 0.10	60%	80%	45%
38		7.0 ± 0.09	53%	70%	70%
39		6.2 ± 0.09	N.D.	N.D.	N.D.
40		7.2 ± 0.02	53%	67%	65%
41		7.0 ± 0.05	54%	75%	36%
42		6.9 ± 0.02	55%	74%	78%

^aPotency was expressed as pIC₅₀(M) ± SEM. ^bStability was expressed by % compound remaining after incubation (120 min).

Scheme 3. Synthesis of 43^a

^aReagents and conditions: (a) *p*-fluorobenzyl chloride, K₂CO₃, DMF, rt; (b) NBS, TsOH, CH₃CN, 80 °C; (c) formamide, 160 °C; (d) *p*-nitrophenylchloroformate, Et₃N, DMF, 0 °C; (e) 4-phenylbutan-1-amine, Et₃N, DCM.

and subsequent cyclization with formamide to yield the fluorobenzylether derivative 45. Finally, urea synthesis was completed using *p*-nitrophenylchloroformate and 4-phenylbutan-1-amine to provide 43.

Encouragingly, 43 demonstrated higher potency than 30 as well as significantly improving mouse microsomal stability (Table 4). In addition, 43 demonstrated higher stability than our benchmark compound, carmofur (9) (43% vs 28%) (Table 4).

Given the promising parameters of 43, we next compared its potency to carmofur. 43 demonstrated greater potency than carmofur in enzymatic as well as A375 melanoma cell assay (Figure 3A). Based on these results, we proceeded to test compound 43 in cell-based assays, including those using HSCs. We employed the aCDase activity assay using RBM 14–12 in melanoma A375 cells. We observed that 43 demonstrated reasonable potency in this assay (pIC₅₀ = 6.8) (Figures 3B). We then tested 43 in human hepatic stellate cells (HSCs), which are the primary cell type responsible for fibrogenesis. We confirmed that 43 significantly decreases aCDase enzymatic activity as measured in HSC lysate (Figures 3C). In their quiescent state, HSCs store lipid droplets; in response to chronic injury, HSCs undergo activation, leading to production of contractile filaments and extracellular matrix proteins such as alpha-1 smooth muscle actin (encoded by ACTA2) and type I collagen (encoded by COL1A1), respectively. 43 promotes HSC inactivation, as measured by a dose-dependent reduction in COL1A1 and ACTA2 (Figure 3D).

We previously demonstrated that aCDase inhibition with the tool inhibitor B13 (4) or depletion with siRNA promoted HSC inactivation.⁷ Our work further revealed that aCDase inhibition promotes HSC inactivation by regulating Hippo-related transcriptional coactivators Yes-associated protein/transcriptional coactivator with PDZ-binding motif (YAP/TAZ). YAP/TAZ signaling is a core pathway that promotes fibrosis in multiple organs, including the lung, liver, kidney and skin.^{46–50} The transcriptional activity of YAP/TAZ is influenced by their localization in the nucleus or cytoplasm: when localized to the nucleus, YAP/TAZ drive a transcriptional program to drive fibrosis. We observed that B13 (4) inhibits YAP/TAZ activity as measured by a decrease in YAP/TAZ nuclear localization.⁸

Here, we analyzed the efficacy of 43 on YAP/TAZ activity in HSCs. Consistent with our prior results, we observed that 43 significantly inhibited YAP/TAZ nuclear localization (Figure 3E). Importantly, 43 exerted this effect at a much lower dose than B13 (4) (86 nM vs 75 μM), suggesting an increased potency of 43.

Furthermore, we measured the effect of 43 on cell viability. We observed that 43 does not decrease HSC viability in contrast to B13 (4) (Figure 3F). We selected doses of B13 (4) that had been validated in our prior studies with HSCs.^{7,8} We also measured the impact of viability on hepatocytes, which are the most abundant cell type in the liver and play a critical role in various processes including detoxification, metabolism, and protein synthesis. We observed that 43 does not decrease hepatocyte viability even at 4× IC₅₀ in contrast to B13 (4) (Figure 3G). This suggests that compound 43 is nontoxic relative to compound B13 (4), possibly due to its high potency, which allows for effective results at a thousand-fold lower dose. However, its limited kinetic solubility (0.03 μM) precluded further evaluation in an oral PK study.

In addition, we measured the time-dependence of aCDase inactivation by 43 (Figure 4A) to obtain K_{inact}/K_i as $1.68 \times 10^4 \text{ M}^{-1} \text{ s}^{-1}$ (Figure 4B). The linearity observed in k_{obs} -inhibitor plot (Figure 4B) indicates the initial binding event is weak⁵¹ and K_i is presumably higher than 200 nM. Michaelis–Menten

Table 4. In Vitro Potency and Stability Data of 43

ID	pIC ₅₀ Enzymatic	pIC ₅₀ Cellular (A375)	Stability (% remaining)				
			pH = 4.5 (after 120 min)	pH = 7.4 (after 120 min)	5 mM GSH (after 120 min)	Mouse plasma (after 60 min)	Mouse liver microsome (after 45 min)
Camofur (9)	7.6 ± 0.03	6.2 ± 0.09	99%	99%	99%	87%	28%
30	7.9 ± 0.04	Not tested	98%	100%	98%	76%	1%
43	8.5 ± 0.09	6.8 ± 0.07	99%	99%	99%	71%	43%

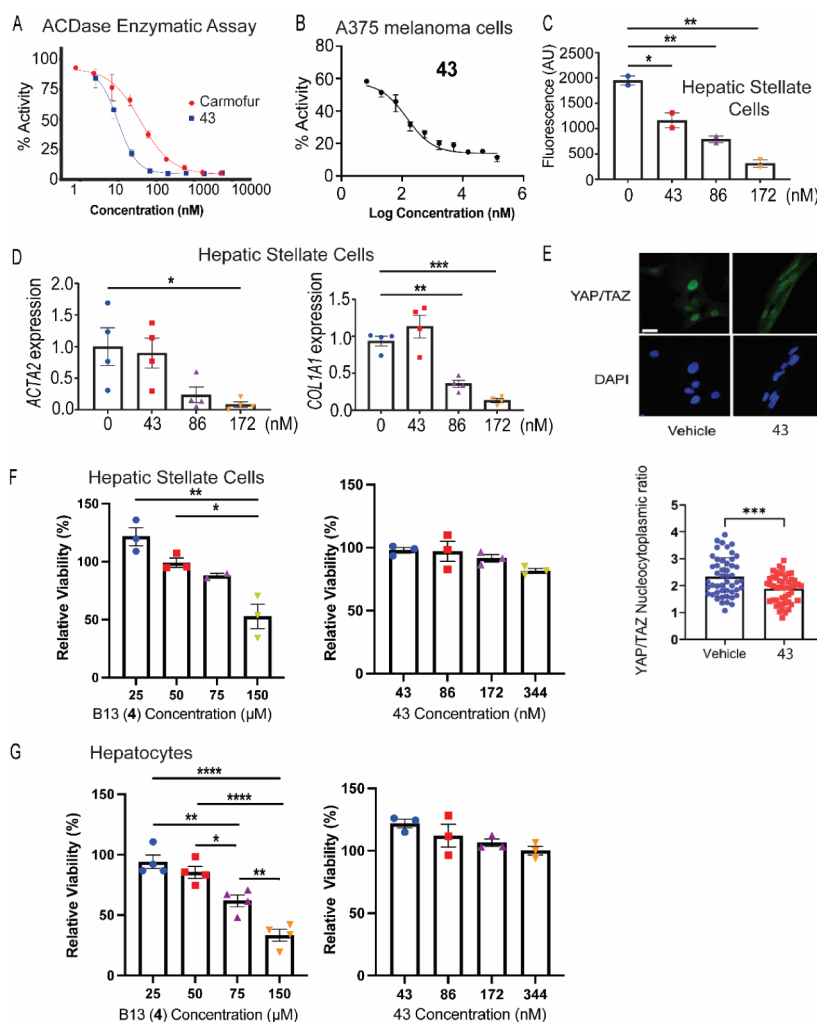


Figure 3. 43 inhibits aCDase enzymatic activity, HSC activation, and YAP/TAZ activity. (A) aCDase enzymatic activity measured using recombinant aCDase enzyme with addition of camofur (9) and 43 at the indicated doses. (B) A375 melanoma cells were treated with 43 at the indicated doses for 2 h and aCDase enzymatic activity was measured. (C) Human hepatic stellate cells were treated with 43 at the indicated doses for 3 h. aCDase enzymatic activity was measured from the HSC lysates. (D) HSCs were treated with DMSO vehicle or 43 at the indicated doses for 48 h. qRT-PCR quantified expression of the indicated genes, and samples were normalized to *GAPDH*. (E) HSCs were treated with DMSO vehicle or 43 (86 nM) for 3 h. Immunofluorescence with anti-YAP/TAZ antibody (top, green) and DAPI (bottom, blue). Scale bar: 25 μ m. Quantification of YAP/TAZ N/C ratio was performed for 50 cells per condition. (F) HSC cells. (G) HepG2 cells were treated with B13 (4) or 43 at the indicated doses for 2 h. Viability was measured using CyQuant Proliferation assay and normalized to viability of vehicle treated cells. Data are expressed as mean \pm SEM. Subsequent statistical analysis was performed with one-way ANOVA with Tukey's method for multiple comparisons. (* $p < 0.05$, ** $p < 0.01$, *** $p < 0.001$, **** $p < 0.0001$).

analysis of aCDase inactivation by 43 also showed decrease in V_{\max} supports covalent mode of aCDase inhibition as observed by others^{36,40} (Figure S25). Further experiments are in progress to elucidate the mechanism of aCDase inactivation. We also performed preliminary proteomics analysis of activated HSCs treated with 43 (Figure 4C). It is noteworthy that several proteins related with Dynein/Kinesin are enriched (NDE1, NDEL1, KIF3B, KIF15) while several proteins

involved with signaling pathway (SARM1, RGAP1, PDGF-D, PDGFR- β) are decreased.

DISCUSSION AND CONCLUSIONS

The potential of aCDase as a therapeutic target in fibrosis and in oncology has been established, but currently, no aCDase inhibitors have received FDA approval or entered clinical trials. The urea scaffold was identified as a crucial structure for these

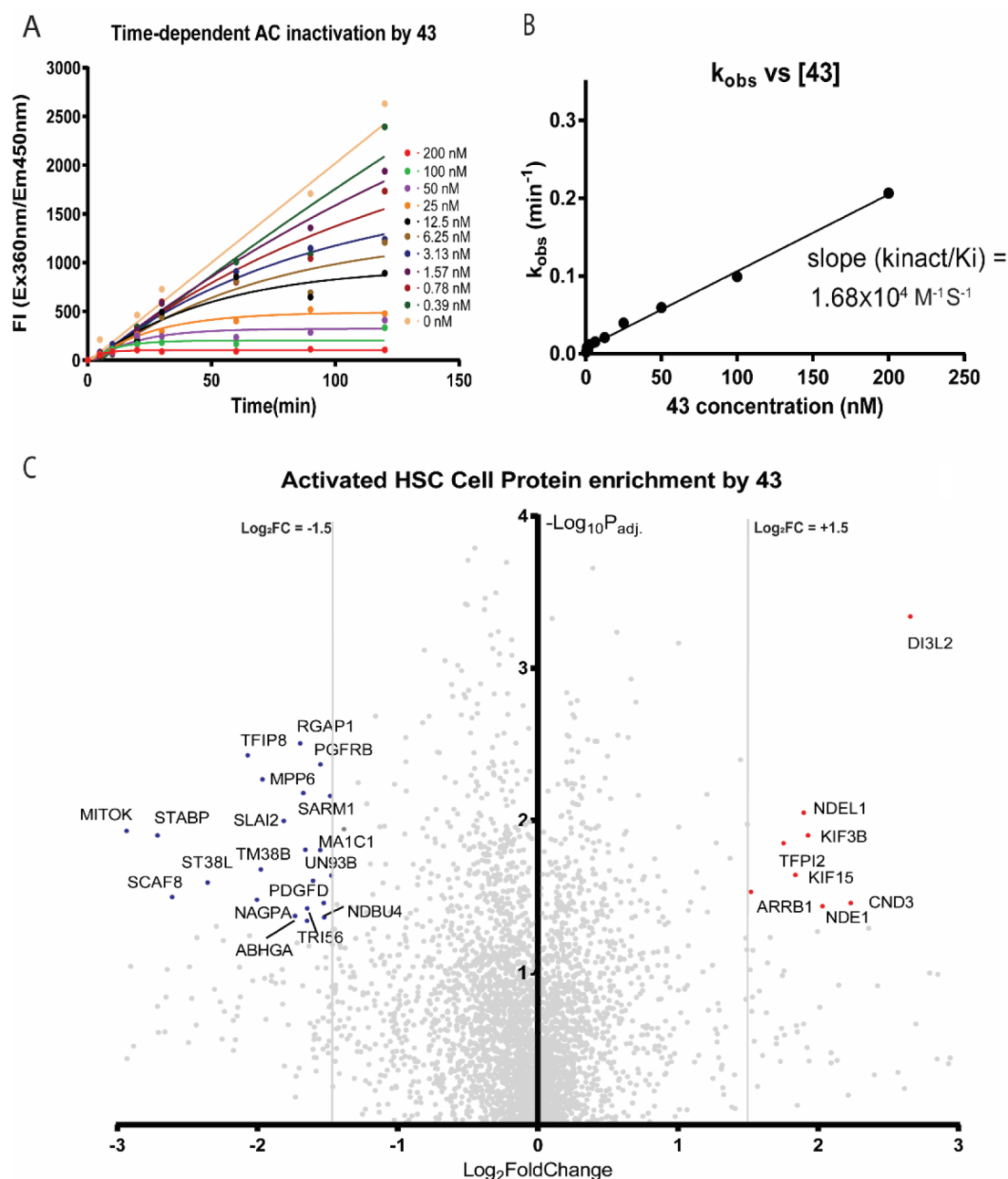


Figure 4. Kinetic and proteomics studies on compound 43 with aCDase. A) Time-dependent inactivation of aCDase was assessed using varying concentrations of inhibitor 43, with aCDase (20 nM) and the substrate RBM14-12 (20 μM). B) Plot of k_{obs} vs inhibitor 43, where k_{obs} values were derived from the progress curves. C) Proteomics analysis of activated HSCs treated with compound 43 (86 nM), with red and blue dots representing proteins that exhibited significant changes in expression levels ($\log_2 \text{Fold Change} > 1.5$ and $p < 0.05$). The vertical gray line indicates the $\log_2 \text{FoldChange}$ cutoff of 1.5.

covalent inhibitors, leading to numerous efforts to optimize in vitro ADME (absorption, distribution, metabolism, and excretion) properties for potential clinical development.

In our search for effective inhibitors, we explored the potential of the phenyl-substituted heteroaryl ring in the urea scaffold to enhance stability. This exploration led to the identification of phenyl-substituted imidazolyl urea as a promising new scaffold. We demonstrated its in vitro potency, particularly in hepatic stellate cells. Among the compounds evaluated, 43 excelled due to its superior potency and chemical stability, making it a strong candidate for further investigation for better solubility and metabolic stability. Interestingly,

although compound 15 (Figure 1B) from a published patent^{1,4} shares a similar scaffold and demonstrates excellent potency ($\text{IC}_{50} = 13 \text{ nM}$), it showed poor stability in the buffer (pH = 7.4) as well as GSH assay, with no remaining compound under standard conditions. We are continuing our medicinal chemistry efforts to further optimize this scaffold, focusing specifically on improving kinetic solubility (ideally, $>50 \mu\text{M}$ in simulated intestinal fluid) and metabolic stability (75% remaining after 45 min incubation). In addition, a proteomics study indicates a variety of biological processes are involved upon treatment with 43. PDGF (platelet-derived growth factor) signaling is notable within the group due to the

presence of decreased platelet-derived growth factor D (PDGF-D) and platelet-derived growth factor receptor beta (PDGFR- β). They are key ligand–receptor partners in the PDGF signaling pathway, which drives cell proliferation, survival, and migration. A reduction in both the growth factor (PDGF-D) and its receptor (PDGFR- β) would most directly impair this signaling axis and have a pronounced impact on downstream pathways (e.g., MAPK, PI3K/AKT).⁵² Further elucidation of PDGFR- β pathway with aCDase inhibition and role of proteins involved with dynein/kinesin might be needed to fully understand the mechanism. While the exact role of dynein/NDE1/NDEL1 in aCDase inhibition requires further study, it is interesting that YAP localization into nucleus requires dynein.^{53,54} One limitation of our studies is that the primary enzymatic screening for aCDase inhibition was conducted with a short incubation period (less than 2 hours), which may have resulted in overlooking promising scaffolds with slower reaction kinetics. Further studies are needed to elucidate the role of aCDase inhibition in the broader context of ceramide metabolism during fibrosis. In summary, our study demonstrates that phenyl-substituted imidazolyl urea is a promising scaffold for developing aCDase inhibitors with a favorable balance of potency and stability. Further advancements will be reported in due course.

EXPERIMENTAL SECTION

Chemistry. General Information. All evaporations were carried out *in vacuo* with a rotary evaporator. Analytical samples were dried *in vacuo* (1–5 mmHg) at rt. Thin layer chromatography (TLC) was performed on silica gel plates, spots were visualized by UV light (214 and 254 nm). Purification by column and flash chromatography was carried out using silica gel (200–300 mesh). Solvent systems are reported as mixtures by volume. All NMR spectra were recorded on a Bruker 400 (400 MHz) spectrometer. ¹H chemical shifts are reported in δ values in ppm with the deuterated solvent as the internal standard. Data are reported as follows: chemical shift, multiplicity (s = singlet, d = doublet, t = triplet, q = quartet, br = broad, m = multiplet), coupling constant (Hz), integration. LC–MS spectra were obtained on an Agilent 1200 series 6110 or 6120 mass spectrometer with electrospray ionization and excepted as otherwise indicated, the general LC–MS condition was as follows: Waters X Bridge C18 column (50 mm \times 4.6 mm \times 3.5 μ m), flow rate: 2.0 mL/min, the column temperature: 40 °C. All compounds are >95% pure by HPLC analysis.

Syntheses of Compounds. The Synthesis of *N*-Hexyl-4-phenyl-1*H*-imidazole-1-carboxamide (17). To a stirred solution of 5-phenyl imidazole (300 mg, 2.08 mmol) in pyridine (5 mL) was added DMAP (26 mg, 0.21 mmol) and *n*-hexylisocyanate (238 mg, 1.87 mmol), and this mixture was allowed to stir at 80 °C for 1 h under N₂. After the reaction was completed (by LC–MS), the mixture was concentrated under reduced pressure and dissolved in EtOAc (20 mL). The residue was washed with water and brine, dried over anhydrous Na₂SO₄, filtered and evaporated under reduced pressure. The crude was purified by silica gel chromatography (50% EtOAc in hexane) to give **17** (87 mg, yield: 15%) as a white solid. ¹H NMR (400 MHz, DMSO-*d*₆) 8.20 (t, *J* = 5.6 Hz, 1H), 8.31 (d, *J* = 1.2 Hz, 1H), 8.13 (d, *J* = 1.2 Hz, 1H), 7.80–7.82 (m, 2H), 7.38–7.42 (m, 2H), 7.25–7.29 (m, 1H), 3.24–3.32 (m, 2H), 1.52–1.59 (m, 2H), 1.23–1.37 (m, 6H), 0.86 (t, *J* = 6.8 Hz, 3H). LC–MS *m/z*: 272.3 [*M* + *H*]⁺.

The Synthesis of *N*-Hexyl-2-oxo-5-phenyloxazole-3(2*H*)-carboxamide (18). To a stirred solution of 5-phenyloxazol-2(3*H*)-one (98 mg, 0.61 mmol)⁴⁰ in pyridine (3 mL) was added DMAP (7 mg, 0.06 mmol) and 1-isocyanatohexane (70 mg, 0.55 mmol), and this mixture was allowed to stir at 80 °C for 1 h. After the reaction was completed (by LC–MS), the mixture was concentrated under reduced pressure and dissolved in EtOAc (20 mL). The residue was washed with water and brine, dried over anhydrous Na₂SO₄, filtered and evaporated under reduced pressure. The crude was purified by silica gel chromatography (20–33% EtOAc in hexane) to give **18** (46 mg, yield: 26%) as a white solid. ¹H NMR (400 MHz, CDCl₃) δ 7.95 (br, 1H), 7.51–7.54 (m, 2H), 7.47 (s, 1H), 7.40–7.44 (m, 2H), 7.34–7.38 (m, 1H), 3.37–3.42 (m, 2H), 1.56–1.65 (m, 2H), 1.25–1.41 (m, 6H), 0.90 (t, *J* = 6.8 Hz, 3H). LC–MS *m/z*: 289.1 [*M* + *H*]⁺.

The Synthesis of 4-(2-(Benzyloxy)phenyl)-*N*-hexyl-1*H*-imidazole-1-carboxamide (19). To a solution of 3-phenyl-1*H*-pyrrole⁵⁵ (200 mg, 1.40 mmol) in THF (10 mL), was added NaH (60%, 56 mg, 1.40 mmol) at 0 °C. The reaction mixture was stirred at 0 °C for 10 min then *n*-hexylisocyanate (120 mg, 0.48 mmol) was added, keep the reaction stirring at 0 °C to room temperature over 1 h until the reaction was complete (by LC–MS). Water (20 mL) was added to quench the reaction and the mixture was extracted with EtOAc. The residue was washed with brine, dried over anhydrous Na₂SO₄, filtered and evaporated under reduced pressure. The crude mixture was purified by silica gel chromatography (20–50% EtOAc in hexane) and recrystallized to give **19** (54 mg, yield: 14%) as a white solid.

¹H NMR (400 MHz, CDCl₃) δ 7.52–7.54 (m, 2H), 7.46 (t, *J* = 2.0 Hz, 1H), 7.34–7.38 (m, 2H), 7.22–7.24 (m, 1H), 7.21–7.22 (m, 1H), 6.59–6.60 (m, 1H), 5.48 (br, 1H), 3.41–3.46 (m, 2H), 1.60–1.66 (m, 2H), 1.31–1.39 (m, 6H), 0.90 (t, *J* = 6.8 Hz, 3H). LC–MS *m/z*: 271.2 [*M* + *H*]⁺.

The Synthesis of *N*-Hexyl-4-phenyl-1*H*-pyrazole-1-carboxamide (20). To a stirred solution of 4-phenyl-1*H*-pyrazole (150 mg, 1.08 mmol) in pyridine (5 mL) was added DMAP (14 mg, 0.11 mmol) and *n*-hexylisocyanate (120 mg, 0.94 mmol), and this mixture was allowed to stir at room temperature for 1 h under N₂. After the reaction was completed (by LC–MS), the mixture was concentrated under reduced pressure and dissolved in EtOAc (20 mL). The residue was washed with water and brine, dried over anhydrous Na₂SO₄, filtered and evaporated under reduced pressure. The crude was purified by silica gel chromatography (50% EtOAc in hexane) to give **20** (258 mg, yield: 91%) as a white solid.

¹H NMR (400 MHz, DMSO-*d*₆) 8.75 (s, 1H), 8.55 (t, *J* = 6.0 Hz, 1H), 8.27 (d, *J* = 0.4 Hz, 1H), 7.74–7.76 (m, 2H), 7.37–7.41 (m, 2H), 7.25–7.29 (m, 1H), 3.26 (dd, *J* = 13.6 Hz, 6.8 Hz, 2H), 1.53–1.56 (m, 2H), 1.28–1.31 (m, 6H), 0.86 (t, *J* = 6.4 Hz, 3H). LC–MS *m/z*: 272.2 [*M* + *H*]⁺.

The Synthesis of *N*-Hexyl-4-(3-methoxyphenyl)-1*H*-imidazole-1-carboxamide (23). To a stirred solution of 4-(3-methoxyphenyl)-1*H*-imidazole⁵⁶ (200 mg, 1.15 mmol) in CH₂Cl₂ (5 mL), was added pyridine (5 mL), DMAP (15 mg, 0.12 mmol) and *n*-hexylisocyanate (132 mg, 1.03 mmol), and this mixture was allowed to stir at room temperature for 1 h. After the reaction was completed (by LC–MS), the mixture was concentrated under reduced pressure and dissolved in EtOAc (20 mL). The residue was washed with water and brine, dried over anhydrous Na₂SO₄, filtered and evaporated

under reduced pressure. The crude was purified by silica gel chromatography (20–33% EtOAc in hexane) to give **23** (241 mg, yield: 70%) as a yellow solid.

^1H NMR (400 MHz, CDCl_3) δ 8.16 (d, J = 1.2 Hz, 1H), 7.60–7.61 (m, 1H), 7.28–7.35 (m, 3H), 6.83–6.86 (m, 1H), 6.02–6.15 (m, 1H), 3.84 (s, 3H), 3.39–3.45 (m, 2H), 1.58–1.63 (m, 2H), 1.26–1.36 (m, 6H), 0.89 (dd, J = 6.8 Hz, 5.6 Hz, 3H). LC–MS m/z : 302.2 $[\text{M} + \text{H}]^+$.

The Synthesis of 4-(4-Fluorophenyl)-N-Hexyl-1H-imidazole-1-carboxamide (24). To a stirred solution of 4-(4-fluorophenyl)-1H-imidazole (162 mg, 1 mmol) in CH_2Cl_2 (5 mL), was added pyridine (5 mL), DMAP (12 mg, 0.1 mmol) and *n*-hexylisocyanate (115 mg, 0.9 mmol), and this mixture was allowed to stir at room temperature for 1 h. After the reaction was completed (by LC–MS), the mixture was concentrated under reduced pressure and dissolved in EtOAc (20 mL). The residue was washed with water and brine, dried over anhydrous Na_2SO_4 , filtered and evaporated under reduced pressure. The crude was purified by silica gel chromatography (20–33% EtOAc in hexane) to give **24** (58 mg, yield: 20%) as a white solid.

^1H NMR (400 MHz, CDCl_3) δ 8.13 (d, J = 1.2 Hz, 1H), 7.70–7.74 (m, 2H), 7.55 (d, J = 1.2 Hz, 1H), 7.05–7.71 (m, 2H), 5.98 (br, 1H), 3.40–3.45 (m, 2H), 1.59–1.67 (m, 2H), 1.27–1.41 (m, 6H), 0.90 (t, J = 6.8 Hz, 3H). LC–MS m/z : 290.2 $[\text{M} + \text{H}]^+$.

The Synthesis of N-Hexyl-4-(4-Methoxyphenyl)-1H-imidazole-1-carboxamide (25). To a stirred solution of 4-(4-methoxyphenyl)-1H-imidazole⁵⁷ (348 mg, 2.00 mmol) in CH_2Cl_2 (5 mL), was added pyridine (5 mL), DMAP (25 mg, 0.20 mmol) and *n*-hexylisocyanate (229 mg, 1.8 mmol), and this mixture was allowed to stir at room temperature for 2 h. After the reaction was completed (by LC–MS), the mixture was concentrated under reduced pressure and dissolved in EtOAc (20 mL). The residue was washed with water and brine, dried over anhydrous Na_2SO_4 , filtered and evaporated under reduced pressure. The crude was purified by silica gel chromatography (20–33% EtOAc in hexane) to give **25** (36 mg, yield: 6%) as a white solid.

^1H NMR (400 MHz, CDCl_3) δ 8.17 (d, J = 0.8 Hz, 1H), 7.70–7.73 (m, 2H), 7.46 (d, J = 1.2 Hz, 1H), 6.92–6.95 (m, 2H), 5.67 (br, 1H), 3.84 (s, 3H), 3.43–3.49 (m, 2H), 1.62–1.68 (m, 2H), 1.31–1.41 (m, 6H), 0.90 (dd, J = 14.0 Hz, 7.2 Hz, 3H). LC–MS m/z : 302.2 $[\text{M} + \text{H}]^+$.

The Synthesis of 4-(2-Chlorophenyl)-N-hexyl-1H-imidazole-1-carboxamide (26). To a stirred solution of 4-(2-chlorophenyl)-1H-imidazole (200 mg, 1.12 mmol) in CH_2Cl_2 (5 mL), was added pyridine (5 mL), DMAP (14 mg, 0.11 mmol) and *n*-hexylisocyanate (128 mg, 1.01 mmol), and this mixture was allowed to stir at room temperature for 1 h. After the reaction was completed (by LC–MS), the mixture was concentrated under reduced pressure and dissolved in EtOAc (20 mL). The residue was washed with water and brine, dried over anhydrous Na_2SO_4 , filtered and evaporated under reduced pressure. The crude was purified by silica gel chromatography (20–33% EtOAc in hexane) to give **18** (69 mg, yield: 20%) as yellow oil.

^1H NMR (400 MHz, CDCl_3) δ 8.21 (d, J = 1.2 Hz, 1H), 8.11–8.14 (m, 1H), 7.80 (d, J = 1.2 Hz, 1H), 7.41–7.44 (m, 1H), 7.32–7.36 (m, 1H), 7.20–7.26 (m, 1H), 5.97 (br, 1H), 3.40–3.46 (m, 2H), 1.60–1.68 (m, 2H), 1.25–1.41 (m, 6H), 0.91 (t, J = 4.0 Hz, 3H). LC–MS m/z : 290.2 $[\text{M} + \text{H}]^+$

The Synthesis of N-Hexyl-4-(4-hydroxyphenyl)-1H-imidazole-1-carboxamide (27). To a stirred solution of **30** (115 mg, 0.30 mmol), Pd/C (10% palladium on activated carbon, 30 mg) in EtOAc (10 mL) was stirred at room temperature for 2 h under H_2 balloon (1.0 atm) until the reaction was completed (by LC–MS). The reaction mixture was filtered via a pad of Celite and the filtrate was concentrated then purified by preparative HPLC to give **27** (79 mg, yield: 90%) as a white solid.

^1H NMR (400 MHz, $\text{DMSO}-d_6$) δ 9.48 (d, J = 3.2 Hz, 1H), 8.45 (t, J = 5.2 Hz, 1H), 8.23 (d, J = 1.2 Hz, 1H), 7.92 (d, J = 0.8 Hz, 1H), 7.60 (d, J = 8.8 Hz, 2H), 6.78 (d, J = 8.4 Hz, 2H), 3.22–3.27 (m, 2H), 1.51–1.56 (m, 2H), 1.30–1.34 (m, 6H), 0.87 (t, J = 6.4 Hz, 3H). LC–MS m/z : 288.3 $[\text{M} + \text{H}]^+$.

The Synthesis of N-Hexyl-4-*p*-tolyl-1H-imidazole-1-carboxamide (28). To a stirred solution of 4-(4-methylphenyl)-imidazole (200 mg, 1.26 mmol) in CH_2Cl_2 (5 mL), was added pyridine (5 mL), DMAP (16 mg, 0.13 mmol) and *n*-hexylisocyanate (145 mg, 1.14 mmol), and this mixture was allowed to stir at room temperature for 1 h. After the reaction was completed (by LC–MS), the mixture was concentrated under reduced pressure and dissolved in EtOAc (20 mL). The residue was washed with water and brine, dried over anhydrous Na_2SO_4 , filtered and evaporated under reduced pressure. The crude was purified by silica gel chromatography (20–33% EtOAc in hexane) to give **28** (91 mg, yield: 25%) as a white solid.

^1H NMR (400 MHz, CDCl_3) δ 8.15 (d, J = 1.6 Hz, 1H), 7.67 (d, J = 8.4 Hz, 2H), 7.52 (d, J = 1.2 Hz, 1H), 7.20 (d, J = 8.0 Hz, 2H), 5.70 (br, 1H), 3.42–3.47 (m, 2H), 2.37 (s, 3H), 1.61–1.68 (m, 2H), 1.31–1.41 (m, 6H), 0.89 (t, J = 6.8 Hz, 3H). LC–MS m/z : 386.2 $[\text{M} + \text{H}]^+$.

The Synthesis of N-Hexyl-4-(2-hydroxyphenyl)-1H-imidazole-1-carboxamide (29). To a stirred solution of 4-(2-(benzyloxy)phenyl)-1H-imidazole⁵⁸ (120 mg, 0.48 mmol) in pyridine (5 mL) was added DMAP (7 mg, 0.06 mmol) and *n*-hexylisocyanate (57 mg, 0.45 mmol), and this mixture was allowed to stir at room temperature for 4 h. After the reaction was completed (by LC–MS), the mixture was concentrated under reduced pressure and dissolved in EtOAc (20 mL). The residue was washed with water and brine, dried over anhydrous Na_2SO_4 , filtered and evaporated under reduced pressure. The crude was purified by silica gel chromatography (20–50% EtOAc in hexane) get *O*-benzyl protected compound (165 mg, yield: 91%) as a white solid.

^1H NMR (400 MHz, CDCl_3) δ 8.25 (dd, J = 7.6 Hz, J = 1.6 Hz, 1H), 8.22 (d, J = 1.2 Hz, 1H), 7.63 (d, J = 1.2 Hz, 1H), 7.52–7.54 (m, 2H), 7.39–7.46 (m, 3H), 7.26–7.30 (m, 1H), 7.08–7.12 (m, 1H), 7.05 (d, J = 8.0 Hz, 1H), 5.19 (s, 2H), 5.13 (br, 1H), 3.31–3.36 (m, 2H), 1.15–1.55 (m, 2H), 1.32–1.44 (m, 6H), 0.92 (t, J = 6.8 Hz, 3H). LC–MS m/z : 378.1 $[\text{M} + \text{H}]^+$. To a stirred solution of above compound (140 mg, 0.37 mmol), Pd/C (10% palladium on activated carbon, 30 mg) in EtOAc (10 mL) was stirred at room temperature for 2 h under H_2 balloon (1.0 atm) until the reaction was completed (by LC–MS). The reaction mixture was filtered via a pad of Celite and the filtrate was concentrated then purified by preparative HPLC to give **29** (51 mg, yield: 48%) as a white solid.

^1H NMR (400 MHz, $\text{DMSO}-d_6$) δ 10.65 (s, 1H), 8.62 (t, J = 5.2 Hz, 1H), 8.36 (d, J = 1.6 Hz, 1H), 8.17 (d, J = 1.2 Hz, 1H), 7.87 (dd, J = 7.6 Hz, J = 1.6 Hz, 1H), 7.09–7.13 (m, 1H), 6.90–6.92 (m, 1H), 6.84–6.88 (m, 1H), 3.24–3.28 (m,

2H), 1.54–1.58 (m, 2H), 1.29–1.35 (m, 6H), 0.87 (t, $J = 6.8$ Hz, 3H). LC–MS m/z : 288.2 $[M + H]^+$.

The Synthesis of 4-(4-(Benzyloxy)phenyl)-N-Hexyl-1H-imidazole-1-carboxamide (30). To a stirred solution of 4'-benzyloxyacetophenone (1.09 g, 4.8 mmol) in CH_3CN (30 mL) was added TsOH (90 mg, 0.5 mmol) and NBS (855 mg, 4.8 mmol), and this mixture was heated to 80 °C for 9 h. After the reaction was completed (by LC–MS), the mixture was concentrated under reduced pressure and dissolved in EtOAc (50 mL). The residue was washed with water and brine, dried over anhydrous Na_2SO_4 , filtered and evaporated under reduced pressure. The crude was purified by prep-HPLC to give the bromide (780 mg, yield: 53%) as a white solid. stirred solution of the bromide (400 mg, 1.31 mmol) in formamide (5 mL) was heated to 160 °C for 4 h. Then the reaction mixture was poured into water (20 mL), extracted with EtOAc, the combined organic layer was washed with water and brine, dried over anhydrous Na_2SO_4 , filtered and evaporated under reduced pressure. The crude was purified by silica gel chromatography (5–20% MeOH in CH_2Cl_2) to get 4-(4-(benzyloxy)phenyl)-1H-imidazole (310 mg, yield: 95%) as a pink solid. To a stirred solution of 4-(4-(benzyloxy)phenyl)-1H-imidazole (150 mg, 0.60 mmol) in pyridine (5 mL) was added DMAP (7 mg, 0.06 mmol) and *n*-hexylisocyanate (69 mg, 0.54 mmol), and this mixture was allowed to stir at room temperature for 4 h. After the reaction was completed (by LC–MS), the mixture was concentrated under reduced pressure and dissolved in EtOAc (20 mL). The residue was washed with water and brine, dried over anhydrous Na_2SO_4 , filtered and evaporated under reduced pressure. The crude mixture was purified by silica gel chromatography (20–33% EtOAc in hexane) and recrystallized with EtOAc and hexane to give **30** (17 mg, yield: 13%) as a white solid.

^1H NMR (400 MHz, CDCl_3) δ 8.27 (s, 1H), 7.71 (d, $J = 8.8$ Hz, 2H), 7.41–7.47 (m, 3H), 7.38 (t, $J = 8.8$ Hz, 2H), 7.31–7.33 (m, 1H), 7.00–7.03 (m, 2H), 5.78 (t, $J = 1.2$ Hz, 1H), 5.10 (s, 2H), 3.43–3.49 (m, 2H), 1.62–1.70 (m, 2H), 1.31–1.42 (m, 6H), 0.91 (t, $J = 6.8$ Hz, 3H). LC–MS m/z : 378.1 $[M + H]^+$.

The Synthesis of 4-(3-Chlorophenyl)-N-hexyl-1H-imidazole-1-carboxamide (31). To a stirred solution of 4-(3-chlorophenyl)-1H-imidazole⁵⁹ (200 mg, 1.12 mmol) in CH_2Cl_2 (5 mL), was added pyridine (5 mL), DMAP (14 mg, 0.11 mmol) and *n*-hexylisocyanate (128 mg, 1.01 mmol), and this mixture was allowed to stir at room temperature for 1 h. After the reaction was completed (by LC–MS), the mixture was concentrated under reduced pressure and dissolved in EtOAc (20 mL). The residue was washed with water and brine, dried over anhydrous Na_2SO_4 , filtered and evaporated under reduced pressure. The crude was purified by silica gel chromatography (20–33% EtOAc in hexane) to give **31** (271 mg, yield: 79%) as a white solid.

^1H NMR (400 MHz, CDCl_3) δ 8.14 (d, $J = 1.2$ Hz, 1H), 7.74 (t, $J = 1.2$ Hz, 1H), 7.60–7.62 (m, 2H), 7.28–7.32 (m, 1H), 7.24–7.27 (m, 1H), 6.11 (t, $J = 5.2$ Hz, 1H), 3.40–3.45 (m, 2H), 1.59–1.66 (m, 2H), 1.27–1.40 (m, 6H), 0.89 (t, $J = 6.8$ Hz, 3H). LC–MS m/z : 306.1 $[M + H]^+$.

The Synthesis of 4-(4-Fluorophenyl)-N-(4-phenylbutyl)-1H-imidazole-1-carboxamide (33). A mixture of 4-(4-fluorophenyl)-1H-imidazole **32** (162 mg, 1.00 mmol) and TEA (404 mg, 4.00 mmol) in CH_2Cl_2 (20 mL) was added 4-nitrophenyl chloroformate (222 mg, 1.10 mmol), and the reaction mixture was stirred at 0 °C for 1 h. 4-phenylbutan-1-

amine (164 mg, 1.10 mmol) was added to the reaction, the mixture was stirred at room temperature for another 2 h. After the reaction was completed (by LCMS), the mixture was treated with brine (50 mL) and extracted with CH_2Cl_2 (100 mL \times 2), dried over anhydrous sodium sulfate, concentrated in vacuo to give the crude product, then it was purified by column chromatography to give **33** (52 mg, yield: 15%) as a white solid.

^1H NMR (400 MHz, CDCl_3) δ 8.53 (s, 1H), 8.29 (d, $J = 1.2$ Hz, 1H), 8.11 (d, $J = 1.2$ Hz, 1H), 7.81–7.85 (m, 2H), 7.17–7.30 (m, 7H), 3.27–3.32 (m, 2H), 2.51–2.64 (m, 2H), 1.55–1.66 (m, 4H). LC–MS m/z : 338.1 $[M + H]^+$.

N-(3-Chlorophenethyl)-4-(4-fluorophenyl)-1H-imidazole-1-carboxamide (34). Prepared in a similar manner to the synthesis of **33** using 2-(3-chlorophenyl)ethanamine to give **34** (yield: 18%) as a white solid.

^1H NMR (400 MHz, CDCl_3) δ 8.09 (d, $J = 0.8$ Hz, 1H), 7.71–7.75 (m, 2H), 7.45 (d, $J = 0.8$ Hz, 1H), 7.24–7.30 (m, 3H), 7.06–7.13 (m, 3H), 5.75 (s, 1H), 3.68–3.73 (m, 2H), 2.96 (d, $J = 6.8$ Hz, 2H). LC–MS m/z : 344.0 $[M + H]^+$.

4-(4-Fluorophenyl)-N-(3-(4-fluorophenyl)propyl)-1H-imidazole-1-carboxamide (35). Prepared in a similar manner to the synthesis of **33** using 3-(4-fluorophenyl)propan-1-amine to give **35** (yield: 43%) as a white solid.

^1H NMR (400 MHz, CDCl_3) δ 8.07 (d, $J = 1.6$ Hz, 1H), 7.70–7.74 (m, 2H), 7.36 (d, $J = 1.2$ Hz, 1H), 7.15–7.19 (m, 2H), 7.06–7.10 (m, 2H), 6.98–7.03 (m, 2H), 5.70 (t, $J = 5.2$ Hz, 1H), 3.46–3.51 (m, 2H), 2.70–2.74 (m, 2H), 1.95–2.05 (m, 2H). LC–MS m/z : 342.1 $[M + H]^+$.

4-(4-Fluorophenyl)-N-(4-methylbenzyl)-1H-imidazole-1-carboxamide (36). Prepared in a similar manner to the synthesis of **33** using *p*-tolylmethanamine to give **36** (yield: 24%) as a white solid.

^1H NMR (400 MHz, CDCl_3) δ 8.15 (d, $J = 1.2$ Hz, 1H), 7.70–7.74 (m, 2H), 7.51 (d, $J = 1.2$ Hz, 1H), 7.19–7.27 (m, 4H), 7.04–7.12 (m, 2H), 5.92 (s, 1H), 4.58 (d, $J = 5.6$ Hz, 2H), 2.36 (s, 3H). LC–MS m/z : 310.1 $[M + H]^+$.

N-(Cyclopropylmethyl)-4-(4-fluorophenyl)-1H-imidazole-1-carboxamide (37). Prepared in a similar manner to the synthesis of **33** using cyclopropylmethanamine to give **37** (61 mg, yield: 26%) as a white solid.

^1H NMR (400 MHz, CDCl_3) δ 8.18 (d, $J = 1.2$ Hz, 1H), 7.74–7.78 (m, 2H), 7.55 (d, $J = 1.2$ Hz, 1H), 7.07–7.11 (m, 2H), 5.79 (br, 1H), 3.01–3.34 (m, 2H), 1.09–1.13 (m, 1H), 0.60–0.65 (m, 2H), 0.31–0.34 (m, 2H). LC–MS m/z : 260.2 $[M + H]^+$.

(R)-4-(4-Fluorophenyl)-N-(pentan-2-yl)-1H-imidazole-1-carboxamide (38). Prepared in a similar manner to the synthesis of **33** using (*R*)-pentan-2-amine (HCl salt) to **38** (54 mg, yield: 20%) as a yellow solid.

^1H NMR (400 MHz, CDCl_3) δ 8.16 (d, $J = 0.8$ Hz, 1H), 7.74–7.79 (m, 2H), 7.50–7.52 (m, 1H), 7.06–7.20 (m, 2H), 6.38 (d, $J = 6.4$ Hz, 1H), 4.05–4.12 (m, 1H), 1.51–1.66 (m, 2H), 1.38–1.48 (m, 2H), 1.30 (d, $J = 6.4$ Hz, 3H), 0.97 (t, $J = 7.2$ Hz, 3H). LC–MS m/z : 276.1 $[M + H]^+$.

(S)-4-(4-Fluorophenyl)-N-(pentan-2-yl)-1H-imidazole-1-carboxamide (39). Prepared in a similar manner to the synthesis of **33** using (*S*)-pentan-2-amine (HCl salt) to give **39** (yield: 7%) as a white solid.

^1H NMR (400 MHz, CDCl_3) δ 8.14 (d, $J = 1.2$ Hz, 1H), 7.73–7.78 (m, 2H), 7.51 (d, $J = 1.2$ Hz, 1H), 7.06–7.12 (d, $J = 8.0$ Hz, 1H), 5.37 (d, $J = 8.0$ Hz, 1H), 4.05–4.12 (m, 1H),

1.56–1.63 (m, 2H), 1.38–1.54 (m, 2H), 1.25–1.31 (m, 3H), 0.95–1.25 (m, 3H). LC–MS m/z : 276.1 $[M + H]^+$.

***N*-(Cyclobutylmethyl)-4-(4-fluorophenyl)-1H-imidazole-1-carboxamide (40).** Prepared in a similar manner to the synthesis of **33** using cyclobutylmethanamine to give **40** (yield: 38%) as a white solid.

^1H NMR (400 MHz, CDCl_3) δ 8.14 (d, $J = 1.2$ Hz, 1H), 7.71–7.77 (m, 2H), 7.52 (d, $J = 1.2$ Hz, 1H), 7.05–7.11 (m, 2H), 5.72 (br, 1H), 3.47–3.50 (m, 2H), 2.57–2.65 (m, 1H), 2.09–2.17 (m, 2H), 1.91–2.00 (m, 2H), 1.74–1.81 (m, 2H). LC–MS m/z : 274.1 $[M + H]^+$.

4-(4-Fluorophenyl)-*N*-(3-methylcyclobutyl)-1H-imidazole-1-carboxamide (41). Prepared in a similar manner to the synthesis of **33** using 3-methylcyclobutan-1-amine hydrochloride and the crude product was purified by column chromatography and SFC to give **41** (yield: 11%) as a white solid. No further attempt to identify the relative stereochemistry was made.

41 (major product) ^1H NMR (400 MHz, CDCl_3) δ 8.14 (d, $J = 1.2$ Hz, 1H), 7.73–7.77 (m, 2H), 7.52 (d, $J = 1.2$ Hz, 1H), 7.07–7.11 (m, 2H), 5.72 (d, $J = 6.4$ Hz, 1H), 4.24–4.31 (m, 1H), 2.60–2.67 (m, 2H), 2.11–2.17 (m, 1H), 1.55–1.63 (m, 2H), 1.12 (d, $J = 6.8$ Hz, 3H). LC–MS m/z : 274.0 $[M + H]^+$.

4-(4-Fluorophenyl)-*N*-neopentyl-1H-imidazole-1-carboxamide (42). Prepared in a similar manner to the synthesis of **33** using 2,2-dimethylpropan-1-amine to give **42** (yield: 34%) as a white solid.

^1H NMR (400 MHz, CDCl_3) δ 8.20 (s, 1H), 7.75–7.80 (m, 2H), 7.52 (d, $J = 1.2$ Hz, 1H), 7.07–7.13 (m, 2H), 5.67 (s, 1H), 3.28 (d, $J = 6.4$ Hz, 2H), 1.01 (s, 9H). LC–MS m/z : 276.1 $[M + H]^+$.

The Synthesis of 4-(4-(4-Fluorobenzyloxy)phenyl)-*N*-(4-phenylbutyl)-1H-imidazole-1-carboxamide (43). To a stirred solution of 4'-hydroxyacetophenone **44** (680 mg, 5.0 mmol) in DMF (20 mL) was added K_2CO_3 (1.38 g 10.0 mmol) and 1-(chloromethyl)-4-fluorobenzene (722 mg, 5.0 mmol). The reaction mixture was allowed to stir at room temperature for 3 h. After the reaction finished, water (50 mL) was added, extracted with EtOAc (50 mL), the combined organic layer was washed with brine, dried over anhydrous Na_2SO_4 , filtered and evaporated under reduced pressure. The crude was recrystallized with CH_2Cl_2 /hexane to afford the protected acetophenone (1.09 g, yield: 89%) as a white solid. To a stirred solution of above acetophenone (1.09 g, 4.46 mmol) in CH_3CN (30 mL) was added TsOH (90 mg, 0.5 mmol) and NBS (785 mg, 4.46 mmol). The reaction mixture was heated to 80 °C for 9 h. After the reaction was completed, the mixture was concentrated under reduced pressure and dissolved in EtOAc (50 mL), washed with water and brine, dried over anhydrous Na_2SO_4 , filtered and evaporated under reduced pressure. The crude was purified by prep-HPLC to give the corresponding bromoketone (1.20 g, yield: 83%) as a white solid. A mixture of bromoketone from above (1.00 g, 3.09 mmol) and formamide (5 mL) was heated to 160 °C for 4 h. Then the reaction mixture was poured into water (20 mL), extracted with EtOAc, the combined organic layer was washed with water and brine, dried over anhydrous Na_2SO_4 , filtered and evaporated under reduced pressure. The crude was purified by silica gel chromatography (5–20% MeOH in CH_2Cl_2) to get imidazole **45** (600 mg, yield: 72.3%) as a pink solid. To a solution of imidazole **45** (268 mg, 1 mmol) in CH_2Cl_2 (15 mL) was added *p*-nitrophenylchloroformate (201 mg, 1 mmol) and Et_3N (202 mg, 1 mmol) at 0 °C. The

reaction mixture was stirred for 1 h at 0 °C then 4-phenylbutan-1-amine (149 mg, 1 mmol) was added. After stirring at room temperature for 1 h, the reaction mixture was quenched with water, extracted with EtOAc. The combined organic layer was washed with brine, dried over anhydrous Na_2SO_4 and evaporated under reduced pressure. The crude was purified by silica gel chromatography (50% EtOAc/petroleum ether) to afford **43** (98 mg, yield: 22%) as a white solid.

^1H NMR (400 MHz, CDCl_3) δ 8.12 (d, $J = 1.2$ Hz, 1H), 7.70 (d, $J = 8.4$ Hz, 2H), 7.39–7.45 (m, 3H), 7.27–7.29 (m, 2H), 7.17–7.20 (m, 3H), 7.07 (t, $J = 8.8$ Hz, 2H), 6.99 (d, $J = 8.8$ Hz, 2H), 5.74–5.84 (m, 1H), 5.04 (s, 2H), 3.43–3.74 (m, 2H), 2.67 (t, $J = 6.8$ Hz, 2H), 1.59–1.76 (m, 4H). LC–MS m/z : 444.0 $[M + H]^+$.

Computational Modeling of aCDase with 33. The model of **33** bound to aCDase is derived from the 2.7 Å crystal structure of carmofur (**9**) bound human aCDase (PDB ID: 6MHM).¹⁴ This structure only shows *n*-hexylformamide tail of carmofur (**9**) covalently attached to Cys143. Our models are based on the tetrahedral intermediate, where the oxygen carries a negative charge and the $-\text{CONH}-$ is in trans conformation (6MHM is cis). **33** was docked by hand into the active site and minimized along with a 6 Å shell around the compound. The location of the 4-fluorophenylimidazole (left wing) and phenyl (right wing) were adjusted to provide a consistent explanation of the available structure–activity relationship.

Acid Ceramidase Assay Using Purified aCDase. Purified aCDase (hAC I93V, expressed in High Five insect cells infected with baculovirus and self-activated, following established protocols¹¹ at 20 nM was incubated in NaOAc buffer (25 μL , 25 mM, pH 4.5) at 37 °C for 10 min with varying concentrations of the compound (prepared by 2-fold serial dilutions starting from 5 μM) in DMSO, resulting in a final DMSO concentration of 0.5%. Following this, RBM14-12 (20 μM , 25 μL) was added, and the mixture was further incubated at 37 °C for 90 min. Next, methanol (25 μL) and NaIO_4 buffer (50 μL , 2.5 mg/mL NaIO_4 in 100 mM glycine/NaOH buffer, pH 10.6) were added. After an additional incubation for 120 min at room temperature, fluorescence was measured with excitation at 360 nm and emission at 450 nm.

pH Stability Assay. A DMSO stock solution of the inhibitor was added to a buffer (at pH 4.5 or pH 7.4) to a final concentration of 10 μM . The mixture was incubated at 37 °C for 2 h and the aliquot was taken at 5, 15, 30, 45, 60, and 120 min to measure the amount of the remaining compound by LC–MS.

GSH Stability Assay. Inhibitors were dissolved in DMSO and diluted in 5 mM GSH in phosphate buffer (pH = 7.4) to a final concentration of 100 μM . The reaction mixture was incubated at 37 °C for 2 h followed by LC–MS analysis.

Kinetic Solubility Assay. Inhibitors were initially dissolved in DMSO at a concentration of 10 mM and then diluted in 100 mM phosphate buffer (pH 7.4) to a final concentration of 100 μM . The resulting mixture was shaken at room temperature for 1 h (1000 rpm), followed by centrifugation at 12,000 rpm for 10 min to remove any undissolved particles. Aliquots of the supernatant were subsequently analyzed by LC–MS analysis.

Cell Culture. Adult human HSCs isolated from human liver tissue samples were obtained from Triangle Research Laboratories (TRL) as described.⁸

Cells were grown in a humidified 5% CO_2 atmosphere at 37 °C in Dulbecco's Modified Eagle Medium (DMEM with 4.5 g/

L glucose) with 10% fetal bovine serum (FBS), 1% Penicillin/Streptomycin (P/S), and 1% Normocin (ant-nr-1, InvivoGen). Melanoma A375 cells were obtained from ATCC, and grown in Dulbecco's Modified Eagle Medium (DMEM with 4.5 g/L glucose) with 10% fetal bovine serum (FBS). HepG2 cells were obtained from ATCC, and were cultured in DMEM with 4.5 g/L glucose (12800-017, Gibco), Ham's F-12 (21700-075, Gibco) supplemented with 2.4 g/L sodium bicarbonate, 10 mM HEPES, 1% P/S, and 10% FBS.

Immunofluorescence of HSCs. Cells were fixed with 4% paraformaldehyde (Electron Microscopy Sciences) in PBS for 10 min and then blocked in 10% donkey serum (Jackson ImmunoResearch) and 0.1% Triton-100X (BioRad) for 1 h at RT. Cells were incubated with primary antibody diluted in blocking solution overnight at 4 °C. Primary antibodies used were anti-YAP/TAZ (1:500, sc-101199, Santa Cruz) and anti-DYKDDDDK (1:500, PA1-984B, ThermoFisher Scientific). Cells were washed with PBS three times and incubated with Alexa 488 (1:400, ab150073 and ab150105, Abcam) and DAPI (2 µg/mL, D1306, ThermoFisher Scientific) for 1 h at RT. Cells were imaged on the Zeiss LSM 780 confocal microscope at 63× magnification. In each experiment, laser intensity, background level, contrast, and electronic zoom size were collected at the same level. Image processing was performed using Adobe Photoshop software.

Measurement of Nuclear/Cytoplasmic Fluorescence Intensity Ratio. For quantification of YAP/TAZ localization, two mean fluorescence intensity (MFI) measurements were taken per cell utilizing a circular selection of consistent area. One MFI measurement was taken within the nucleus, as identified by DAPI staining, and one within the cytoplasm. A nuclear to cytoplasmic ratio (N/C ratio) was generated per cell. Quantification of images was conducted using ImageJ in a blinded fashion.

Quantitative PCR Analysis. RNA was isolated from HSCs using Trizol Reagent (Life Technologies).⁸ RNA was reverse transcribed with SuperScript IV VILO Master Mix (11756050, Invitrogen). SYBR Green qPCR master mix (B21202, Selleck Chemicals) was used for quantification of cDNA on a QuantStudio 6 Flex Real-Time PCR System (Life Technologies).

We used the following primers: forward *GAPDH* 5'-ACAACCTTTGGTATCGTGGAAGG-3', and reverse *GAPDH* 5'-GCCATCACGCCACAGTTTC-3', forward *COL1A1*, 5'-CAGGCTGGTGTGATGGGATT-3', reverse *COL1A1*, 5'-AGCTCCAGCCTCTCCATCTT-3', forward *ACTA2*, 5'-TCCCATCCATTGTGGGACGT-3', and reverse *ACTA2*, 5'-TTGCTCTGTGCTTCGTCACC-3'.

aCDase Enzymatic Activity Assay. The aCDase activity assay for intact cells and cell lysates was optimized from Bedia et al.⁶⁰ For intact cell assays, A375 melanoma cells (50,000/well) were seeded on 96-well plates in DMEM with 10% FBS. The following day, media was removed and replaced with DMEM with 10% FBS media containing the indicated concentrations of compounds (positive control received DMSO vehicle). Negative control wells contained media but were devoid of cells. Plates were incubated in a humidified 5% CO₂ atm at 37 °C for 2 h. The fluorogenic substrate, RBM 14-12 (ChemPartner), was dissolved in ethanol and added to a final concentration of 20 µM to all wells (125 µL final well volume), and the plates were incubated for 3 h at 37 °C. Finally, the reaction was quenched with 50 µL methanol and 100 µL NaIO₄ (2.5 mg/mL in 0.1 M Glycine-NaOH buffer,

pH 10.6), and the plates were incubated in the dark for 2 h at 37 °C. Fluorescence intensity was measured in a plate reader with excitation at 355 nm and emission at 460 nm. All doses were done in triplicate.

To measure aCDase activity in cell lysates, confluent 10 cm dishes of HSCs were treated with compounds dissolved in DMEM+10%FBS. Cells were incubated for 3 h at 37 °C and then harvested using trypsin/EDTA. After washing thrice with ice-cold PBS, cells were resuspended in 0.2 M sucrose supplemented with 1× Halt protease and phosphatase inhibitor and sonicated on ice (5–10 s). Cell homogenates were centrifuged at 20,000g for 15 min, and the protein concentration in the supernatant was quantified via BCA assay (Thermo Scientific). Next, the enzymatic assay was performed in 96-well plates. Each well contained a mixture of 74.5 µL of 25 mM sodium acetate buffer pH 4.5, 0.5 µL of 4 mM Rbm14-12 substrate solution in ethanol (substrate final concentration 20 µM), and 25 µg of protein in a volume of 25 µL of a 0.2 M sucrose with 1× Halt protease and phosphatase inhibitor solution. Negative control samples consisted of the same incubation mixture in the absence of protein extracts. The plate was incubated at 37 °C for 3 h without agitation. Then, the enzymatic reaction was stopped by adding 50 µL of methanol and 100 µL of 2.5 mg/mL NaIO₄ fresh solution in 0.1 M glycine-NaOH buffer, pH 10.6, to each well. The plate was protected from light and incubated at room temperature for 2 h, and then the released fluorescence was quantified using a microplate fluorescence reader as above.

Cell Viability Assay. HepG2 cells (50,000/well) were seeded onto a 96-well plate in Ham's/DMEM medium. After 24 h, the medium was exchanged with medium containing the compound. Positive control wells received the vehicle for their respective compounds: ethanol for B13 (4) and DMSO for 43, and negative control wells contained no cells. After incubation at 37 °C for 2 h, the CyQUANT NF Cell Proliferation Assay (C7026, Invitrogen) was performed per the manufacturer's instruction. Viability was quantified by normalizing the fluorescence intensity of each compound by the average of the vehicle treated cells.

MS Sample Preparation, Data Acquisition and Search Parameters. HSCs treated compound 43 or ethanol vehicle for 48 h. A total of 4 biological replicates were included per treatment condition. Cells were washed 3× with dPBS prior to pelleting and snap freeze. Stored pellets were then allowed to thaw on ice before preparation with PreOmics iST96 kit with 10 mg/100 mL protease inhibitor cocktail (Sigma-Aldrich). A nanoElute was attached in line to a timsTOF Pro equipped with a CaptiveSpray Source (Bruker, Hamburg, Germany). Chromatography was conducted at 40 °C through a 25 cm reversed-phase C18 column (PepSep) at a constant flow rate of 0.5 µL/min. Mobile phase A was 98/2/0.1% water/MeCN/formic Acid (v/v/v) and phase B was MeCN with 0.1% formic acid (v/v). During a 108 min method, peptides were separated by a 3-step linear gradient (5% to 30% B over 90 min, 30% to 35% B over 10 min, 35% to 95% B over 4 min) followed by a 4 min isocratic flush at 95% for 4 min before washing and a return to low organic conditions. Experiments were run as data-dependent acquisitions with ion mobility activated in PASEF mode. MS and MS/MS spectra were collected with *m/z* 100 to 1700 and ions with *z* = +1 were excluded. Raw data files were searched using PEAKS Online Xpro 1.6 (Bioinformatics Solutions Inc., Waterloo, Ontario, Canada). The precursor mass error tolerance and fragment mass error

tolerance were set to 20 ppm and 0.03 respectively. The trypsin digest mode was set to semispecific and missed cleavages was set to 2. The human Swiss-Prot reviewed (canonical) database (downloaded from UniProt) and the common repository of adventitious proteins (cRAP, downloaded from The Global Proteome Machine Organization) totaling 20,487 entries were used. Carbamidomethylation was selected as a fixed modification. Oxidation (M) was selected as a variable modification.

■ ASSOCIATED CONTENT

Data Availability Statement

The data underlying this study are available in the published article and its [Supporting Information](#).

■ Supporting Information

The Supporting Information is available free of charge at <https://pubs.acs.org/doi/10.1021/acsomega.5c03734>.

¹H NMR spectrum of compounds 17–20, 23–31, and 33–43; LC–MS and ¹H NMR spectrum of compound 43; Michaelis–Menten analysis of compound 43 with aCDase (PDF)

Molecular formula strings (CSV)

■ AUTHOR INFORMATION

Corresponding Author

Hyunil Jo – Department of Pharmaceutical Chemistry, University of California, San Francisco, California 94143, United States; orcid.org/0000-0002-4863-0779; Email: Hyunil.jo@ucsf.edu

Authors

Richard Beresis – Department of Pharmaceutical Chemistry, University of California, San Francisco, California 94143, United States

Vijaya Prathigudupu – Division of Gastroenterology, Department of Medicine, University of California, San Francisco, California 94143, United States

Carson Cable – Division of Gastroenterology, Department of Medicine, University of California, San Francisco, California 94143, United States

Amy Yu – Division of Gastroenterology, Department of Medicine, University of California, San Francisco, California 94143, United States; Present Address: Harvard University, Boston, MA 02115, USA

Marc Adler – ChemPartner, South San Francisco, California 94080, United States

Roopa Ramamoorthi – Innovation Ventures, University of California, San Francisco, California 94143, United States

Seul Ki Yeon – Department of Pharmaceutical Chemistry, University of California, San Francisco, California 94143, United States

John D. Gordan – Division of Hematology and Oncology, University of California, San Francisco, California 94143, United States

Sachin Sharma – Division of Gastroenterology, Department of Medicine, University of California, San Francisco, California 94143, United States

William F. DeGrado – Department of Pharmaceutical Chemistry, University of California, San Francisco, California 94143, United States; orcid.org/0000-0003-4745-263X

Balyn Zaro – Department of Pharmaceutical Chemistry, University of California, San Francisco, California 94143, United States

Jennifer Y. Chen – Division of Gastroenterology, Department of Medicine, University of California, San Francisco, California 94143, United States; Liver Center, University of California San Francisco, San Francisco, California 94143, United States

Complete contact information is available at:

<https://pubs.acs.org/doi/10.1021/acsomega.5c03734>

Author Contributions

R.B., J.Y.C., H.J., and W.F.D. conceptualized the idea, while V.P., C.C., S.S., S.K.Y., and B.Z. conducted the experiments under the supervision of J.Y.C., W.F.D., R.B., and H.J. M.A. performed the computational modeling, and data visualization and analysis were carried out by H.J., J.Y.C., V.P., M.A., and J.G. The manuscript was drafted and reviewed by all authors.

Notes

The authors declare no competing financial interest.

■ ACKNOWLEDGMENTS

We appreciate the editorial suggestions and scientific input by Dean Sheppard (UCSF). Research reported in this publication was supported by the following funding: National Institutes of Health grant R01DK134723 (to J.Y.C.), National Institutes of Health grant R01DK137892 (to H.J., J.Y.C., and W.F.D.), P41GM108538 (to J.J.C.), R35GM122603 (to W.F.D.), Innovation Ventures Philanthropy Fund (to J.Y.C., H.J., and W.F.D.), Harrington Scholar Innovator Award (to J.Y.C.). The content is solely the responsibility of the authors and does not necessarily represent the official views of the NIH.

■ REFERENCES

- (1) Kisseleva, T.; Brenner, D. Molecular and cellular mechanisms of liver fibrosis and its regression. *Nat. Rev. Gastroenterol. Hepatol.* **2021**, *18* (3), 151–166.
- (2) Bataller, R.; Brenner, D. A. Liver fibrosis. *J. Clin. Invest.* **2005**, *115* (2), 209–218.
- (3) Friedman, S. L. Mechanisms of hepatic fibrogenesis. *Gastroenterology* **2008**, *134* (6), 1655–1669.
- (4) Bedossa, P.; Dargere, D.; Paradis, V. Sampling variability of liver fibrosis in chronic hepatitis C. *Hepatology* **2003**, *38* (6), 1449–1457.
- (5) Campana, L.; Esser, H.; Huch, M.; Forbes, S. Liver regeneration and inflammation: from fundamental science to clinical applications. *Nat. Rev. Mol. Cell Biol.* **2021**, *22* (9), 608–624.
- (6) Harrison, S. A.; Bedossa, P.; Guy, C. D.; Schattenberg, J. M.; Loomba, R.; Taub, R.; Labriola, D.; Moussa, S. E.; Neff, G. W.; Rinella, M. E.; et al. A Phase 3, Randomized, Controlled Trial of Resmetirom in NASH with Liver Fibrosis. *N. Engl. J. Med.* **2024**, *390* (6), 497–509.
- (7) Chen, J. Y.; Newcomb, B.; Zhou, C.; Pondick, J. V.; Ghoshal, S.; York, S. R.; Motola, D. L.; Coant, N.; Yi, J. K.; Mao, C.; et al. Tricyclic Antidepressants Promote Ceramide Accumulation to Regulate Collagen Production in Human Hepatic Stellate Cells. *Sci. Rep.* **2017**, *7*, 44867.
- (8) Alsamman, S.; Christenson, S. A.; Yu, A.; Ayad, N. M. E.; Mooring, M. S.; Segal, J. M.; Hu, J. K.; Schaub, J. R.; Ho, S. S.; Rao, V.; et al. Targeting acid ceramidase inhibits YAP/TAZ signaling to reduce fibrosis in mice. *Sci. Transl. Med.* **2020**, *12* (557), No. eaay8798.
- (9) Gatt, S. Enzymic Hydrolysis and Synthesis of Ceramides. *J. Biol. Chem.* **1963**, *238*, 3131–3133.
- (10) Bernardo, K.; Hurwitz, R.; Zenk, T.; Desnick, R. J.; Ferlinz, K.; Schuchman, E. H.; Sandhoff, K. Purification, characterization, and

biosynthesis of human acid ceramidase. *J. Biol. Chem.* **1995**, *270* (19), 11098–11102.

(11) Gebai, A.; Gorelik, A.; Li, Z.; Illes, K.; Nagar, B. Structural basis for the activation of acid ceramidase. *Nat. Commun.* **2018**, *9* (1), 1621.

(12) Mao, C.; Obeid, L. M. Ceramidases: regulators of cellular responses mediated by ceramide, sphingosine, and sphingosine-1-phosphate. *Biochim. Biophys. Acta, Protein Struct. Mol. Enzymol.* **2008**, *1781* (9), 424–434.

(13) Okino, N.; He, X.; Gatt, S.; Sandhoff, K.; Ito, M.; Schuchman, E. H. The reverse activity of human acid ceramidase. *J. Biol. Chem.* **2003**, *278* (32), 29948–29953.

(14) Dementiev, A.; Joachimiak, A.; Nguyen, H.; Gorelik, A.; Illes, K.; Shabani, S.; Gelsomino, M.; Ahn, E. E.; Nagar, B.; Doan, N. Molecular Mechanism of Inhibition of Acid Ceramidase by Carmofur. *J. Med. Chem.* **2019**, *62* (2), 987–992.

(15) Camacho, L.; Meca-Cortés, Ó.; Abad, J. L.; García, S.; Rubio, N.; Díaz, A.; Celià-Terrassa, T.; Cingolani, F.; Bermudo, R.; Fernández, P. L. Acid ceramidase as a therapeutic target in metastatic prostate cancer [S]. *J. Lipid Res.* **2013**, *54* (5), 1207–1220.

(16) Parveen, F.; Bender, D.; Law, S. H.; Mishra, V. K.; Chen, C. C.; Ke, L. Y. Role of Ceramidases in Sphingolipid Metabolism and Human Diseases. *Cells* **2019**, *8* (12), 1573.

(17) Newton, J.; Lima, S.; Maceyka, M.; Spiegel, S. Revisiting the sphingolipid rheostat: Evolving concepts in cancer therapy. *Exp. Cell Res.* **2015**, *333* (2), 195–200.

(18) Zaibaq, F.; Dowdy, T.; Larion, M. Targeting the Sphingolipid Rheostat in Gliomas. *Int. J. Mol. Sci.* **2022**, *23* (16), 9255.

(19) Govindarajah, N.; Clifford, R.; Bowden, D.; Sutton, P. A.; Parsons, J. L.; Vimalachandran, D. Sphingolipids and acid ceramidase as therapeutic targets in cancer therapy. *Crit. Rev. Oncol. Hematol.* **2019**, *138*, 104–111.

(20) Mahdy, A. E.; Cheng, J. C.; Li, J.; Elojeimy, S.; Meacham, W. D.; Turner, L. S.; Bai, A.; Gault, C. R.; McPherson, A. S.; Garcia, N. Acid ceramidase upregulation in prostate cancer cells confers resistance to radiation: AC inhibition, a potential radiosensitizer. *Mol. Ther.* **2009**, *17* (3), 430–438.

(21) Realini, N.; Palese, F.; Pizzirani, D.; Pontis, S.; Basit, A.; Bach, A.; Ganesan, A.; Piomelli, D. Acid ceramidase in melanoma: expression, localization, and effects of pharmacological inhibition. *J. Biol. Chem.* **2016**, *291* (5), 2422–2434.

(22) Tan, S.-F.; Liu, X.; Fox, T. E.; Barth, B. M.; Sharma, A.; Turner, S. D.; Awwad, A.; Dewey, A.; Doi, K.; Spitzer, B. Acid ceramidase is upregulated in AML and represents a novel therapeutic target. *Oncotarget* **2016**, *7* (50), 83208.

(23) Huang, Y.; Tanimukai, H.; Liu, F.; Iqbal, K.; Grundke-Iqbal, I.; Gong, C. X. Elevation of the level and activity of acid ceramidase in Alzheimer's disease brain. *Eur. J. Neurosci.* **2004**, *20* (12), 3489–3497.

(24) Sugita, M.; Williams, M.; Dulaney, J. T.; Moser, H. W. Ceramidase and ceramide synthesis in human kidney and cerebellum. Description of a new alkaline ceramidase. *Biochim. Biophys. Acta, Protein Struct. Mol. Enzymol.* **1975**, *398* (1), 125–131.

(25) Bedia, C.; Canals, D.; Matabosch, X.; Harrak, Y.; Casas, J.; Llebaria, A.; Delgado, A.; Fabriàs, G. Cytotoxicity and acid ceramidase inhibitory activity of 2-substituted aminoethanol amides. *Chem. Phys. Lipids* **2008**, *156* (1–2), 33–40.

(26) Bielawska, A.; Greenberg, M. S.; Perry, D.; Jayadev, S.; Shayman, J. A.; McKay, C.; Hannun, Y. A. (1S, 2R)-D-erythro-2-(N-Myristoylamino)-1-phenyl-1-propanol as an Inhibitor of Ceramidase (*). *J. Biol. Chem.* **1996**, *271* (21), 12646–12654.

(27) Raisova, M.; Goltz, G.; Bektas, M.; Bielawska, A.; Riebeling, C.; Hossini, A. M.; Eberle, J.; Hannun, Y. A.; Orfanos, C. E.; Geilen, C. C. Bcl-2 overexpression prevents apoptosis induced by ceramidase inhibitors in malignant melanoma and HaCaT keratinocytes. *FEBS Lett.* **2002**, *516* (1–3), 47–52.

(28) Draper, J. M.; Xia, Z.; Smith, R. A.; Zhuang, Y.; Wang, W.; Smith, C. D. Discovery and evaluation of inhibitors of human ceramidase. *Mol. Cancer Ther.* **2011**, *10* (11), 2052–2061.

(29) Aseeri, M.; Abad, J. L.; Delgado, A.; Fabriàs, G.; Triola, G.; Casas, J. High-throughput discovery of novel small-molecule inhibitors of acid Ceramidase. *J. Enzyme Inhib. Med. Chem.* **2023**, *38* (1), 343–348.

(30) Camacho, L.; Meca-Cortés, Ó.; Abad, J. L.; García, S.; Rubio, N.; Díaz, A.; Celià-Terrassa, T.; Cingolani, F.; Bermudo, R.; Fernández, P. L. Acid ceramidase as a therapeutic target in metastatic prostate cancer. *J. Lipid Res.* **2013**, *54* (5), 1207–1220.

(31) Muley Vilamu, H.; Dowdy, T.; Zaibaq, F.; Karadimov, G.; Li, A.; Song, H.; Zhang, M.; Zhang, W.; Wong, Z.; Zhang, L. Targeting IDH1-Mutated Oligodendroglioma with Acid Ceramidase Inhibitors. *bioRxiv* **2024**, 2024–04.

(32) Ordóñez, Y. F.; Abad, J. L.; Aseeri, M.; Casas, J.; Garcia, V.; Casasampere, M.; Schuchman, E. H.; Levade, T.; Delgado, A.; Triola, G. Activity-based imaging of acid ceramidase in living cells. *J. Am. Chem. Soc.* **2019**, *141* (19), 7736–7742.

(33) Realini, N.; Solorzano, C.; Pagliuca, C.; Pizzirani, D.; Armirotti, A.; Luciani, R.; Costi, M. P.; Bandiera, T.; Piomelli, D. Discovery of highly potent acid ceramidase inhibitors with in vitro tumor chemosensitizing activity. *Sci. Rep.* **2013**, *3* (1), 1035.

(34) Kuzuhara, S.; Ohkoshi, N.; Kanemaru, K.; Hashimoto, H.; Nakanishi, T.; Toyokura, Y. Subacute leucoencephalopathy induced by carmofur, a 5-fluorouracil derivative. *J. Neurol.* **1987**, *234* (6), 365–370.

(35) Diamanti, E.; Bottegoni, G.; Goldoni, L.; Realini, N.; Pagliuca, C.; Bertozzi, F.; Piomelli, D.; Pizzirani, D. Pyrazole-based acid ceramidase inhibitors: design, synthesis, and structure–activity relationships. *Synthesis* **2016**, *48* (17), 2739–2756.

(36) Di Martino, S.; Tardia, P.; Cilibrasi, V.; Caputo, S.; Mazzonna, M.; Russo, D.; Penna, I.; Realini, N.; Margaroli, N.; Migliore, M. Lead optimization of benzoxazolone carboxamides as orally bioavailable and CNS penetrant acid ceramidase inhibitors. *J. Med. Chem.* **2020**, *63* (7), 3634–3664.

(37) Pizzirani, D.; Bach, A.; Realini, N.; Armirotti, A.; Mengatto, L.; Bauer, I.; Girotto, S.; Pagliuca, C.; De Vivo, M.; Summa, M. Benzoxazolone carboxamides: potent and systemically active inhibitors of intracellular acid ceramidase. *Angew. Chem., Int. Ed.* **2015**, *127* (2), 495–499.

(38) Bach, A.; Pizzirani, D.; Realini, N.; Vozella, V.; Russo, D.; Penna, I.; Melzig, L.; Scarpelli, R.; Piomelli, D. Benzoxazolone carboxamides as potent acid ceramidase inhibitors: synthesis and structure–activity relationship (SAR) studies. *J. Med. Chem.* **2015**, *58* (23), 9258–9272.

(39) Ortega, J. A.; Arencibia, J. M.; La Sala, G.; Borgogno, M.; Bauer, I.; Bono, L.; Braccia, C.; Armirotti, A.; Girotto, S.; Ganesan, A. Pharmacophore identification and scaffold exploration to discover novel, potent, and chemically stable inhibitors of acid ceramidase in melanoma cells. *J. Med. Chem.* **2017**, *60* (13), 5800–5815.

(40) Caputo, S.; Di Martino, S.; Cilibrasi, V.; Tardia, P.; Mazzonna, M.; Russo, D.; Penna, I.; Summa, M.; Bertozzi, S. M.; Realini, N. Design, synthesis, and biological evaluation of a series of oxazolone carboxamides as a novel class of acid ceramidase inhibitors. *J. Med. Chem.* **2020**, *63* (24), 15821–15851.

(41) Skerlj, R. T.; Bourque, E. M. J.; Ray, S.; Lansbury, P. T. *Substituted imidazole carboxamides and their use in the treatment of medical disorders*. World Intellectual Property Organization (WIPO). WO 2,021,055,612 A1, 2021.

(42) Bedia, C.; Camacho, L.; Abad, J. L.; Fabriàs, G.; Levade, T. A simple fluorogenic method for determination of acid ceramidase activity and diagnosis of Farber disease. *J. Lipid Res.* **2010**, *51* (12), 3542–3547.

(43) Rothmund, M.; Bär, A.; Klatt, F.; Weidler, S.; Köhler, L.; Unverzagt, C.; Kuhn, C.-D.; Schobert, R. N-Metalloceonoylsphingosines as targeted ceramidase inhibitors: Syntheses and antitumoral effects. *Bioorg. Chem.* **2020**, *97*, 103703.

(44) Pizzirani, D.; Pagliuca, C.; Realini, N.; Branduardi, D.; Bottegoni, G.; Mor, M.; Bertozzi, F.; Scarpelli, R.; Piomelli, D.; Bandiera, T. Discovery of a new class of highly potent inhibitors of

acid ceramidase: synthesis and structure-activity relationship (SAR). *J. Med. Chem.* **2013**, *56* (9), 3518–3530.

(45) Dementiev, A.; Joachimiak, A.; Nguyen, H.; Gorelik, A.; Illes, K.; Shabani, S.; Gelsomino, M.; Ahn, E.-Y. E.; Nagar, B.; Doan, N. Molecular mechanism of inhibition of acid ceramidase by carmofur. *J. Med. Chem.* **2019**, *62* (2), 987–992.

(46) Liu, F.; Lagares, D.; Choi, K. M.; Stopfer, L.; Marinkovic, A.; Vrbanc, V.; Probst, C. K.; Hiemer, S. E.; Sisson, T. H.; Horowitz, J. C.; et al. Mechanosignaling through YAP and TAZ drives fibroblast activation and fibrosis. *Am. J. Physiol. Lung Cell Mol. Physiol.* **2015**, *308* (4), L344–357.

(47) Szeto, S. G.; Narimatsu, M.; Lu, M.; He, X.; Sidiqi, A. M.; Tolosa, M. F.; Chan, L.; De Freitas, K.; Bialik, J. F.; Majumder, S.; et al. YAP/TAZ Are Mechanoregulators of TGF- β -Smad Signaling and Renal Fibrogenesis. *J. Am. Soc. Nephrol.* **2016**, *27* (10), 3117–3128.

(48) Zhang, K.; Chang, Y.; Shi, Z.; Han, X.; Han, Y.; Yao, Q.; Hu, Z.; Cui, H.; Zheng, L.; Han, T.; et al. omega-3 PUFAs ameliorate liver fibrosis and inhibit hepatic stellate cells proliferation and activation by promoting YAP/TAZ degradation. *Sci. Rep.* **2016**, *6*, 30029.

(49) Mannaerts, I.; Leite, S. B.; Verhulst, S.; Claerhout, S.; Eysackers, N.; Thoen, L. F.; Hoorens, A.; Reynaert, H.; Halder, G.; van Grunven, L. A. The Hippo pathway effector YAP controls mouse hepatic stellate cell activation. *J. Hepatol.* **2015**, *63* (3), 679–688.

(50) He, X.; Tolosa, M. F.; Zhang, T.; Goru, S. K.; Ulloa Severino, L.; Misra, P. S.; McEvoy, C. M.; Caldwell, L.; Szeto, S. G.; Gao, F.; et al. Myofibroblast YAP/TAZ activation is a key step in organ fibrogenesis. *JCI Insight* **2022**, *7* (4), No. e146243.

(51) Tonge, P. J. Quantifying the interactions between biomolecules: guidelines for assay design and data analysis. *ACS Infect. Dis.* **2019**, *5* (6), 796–808.

(52) Zhang, H.; Bajraszewski, N.; Wu, E.; Wang, H.; Moseman, A. P.; Dabora, S. L.; Griffin, J. D.; Kwiatkowski, D. J. PDGFRs are critical for PI3K/Akt activation and negatively regulated by mTOR. *J. Clin. Invest.* **2007**, *117* (3), 730–738.

(53) Garrott, S. R.; Gillies, J. P.; DeSantis, M. E. Nde1 and Ndel1: outstanding mysteries in dynein-mediated transport. *Front. Cell Dev. Biol.* **2022**, *10*, 871935.

(54) You, E.; Ko, P.; Jeong, J.; Keum, S.; Kim, J.-W.; Seo, Y.-J.; Song, W. K.; Rhee, S. Dynein-mediated nuclear translocation of yes-associated protein through microtubule acetylation controls fibroblast activation. *Cell. Mol. Life Sci.* **2020**, *77*, 4143–4161.

(55) Smith, N. D.; Huang, D.; Cosford, N. D. One-step synthesis of 3-aryl- and 3,4-diaryl-(1H)-pyrroles using tosylmethyl isocyanide (TOSMIC). *Org. Lett.* **2002**, *4* (20), 3537–3539.

(56) Kasanen, H.; Myllymaki, M. J.; Minkkila, A.; Katja, A. O.; Saario, S. M.; Nevalainen, T.; Koskinen, A. M.; Poso, A. 3-Heterocycle-phenyl N-alkylcarbamates as FAAH inhibitors: design, synthesis and 3D-QSAR studies. *ChemMedchem* **2010**, *5* (2), 213–231.

(57) Rogacki, M. K.; Pitta, E.; Balabon, O.; Huss, S.; Lopez-Roman, E. M.; Argryrou, A.; Blanco-Ruano, D.; Cacho, M.; Vande Velde, C. M. L.; Augustyns, K.; et al. Identification and Profiling of Hydantoins-A Novel Class of Potent Antimycobacterial DprE1 Inhibitors. *J. Med. Chem.* **2018**, *61* (24), 11221–11249.

(58) Kumar, S.; Waldo, J. P.; Jaipuri, F. A.; Marcinowicz, A.; Van Allen, C.; Adams, J.; Kesharwani, T.; Zhang, X.; Metz, R.; Oh, A. J.; et al. Discovery of Clinical Candidate (1R,4R)-4-((R)-2-((S)-6-Fluoro-5H-imidazo[5,1-a]isindol-5-yl)-1-hydroxyethyl)cyclohexan-1-ol (Navoximod), a Potent and Selective Inhibitor of Indoleamine 2,3-Dioxygenase 1. *J. Med. Chem.* **2019**, *62* (14), 6705–6733.

(59) Rohrig, U. F.; Majjigapu, S. R.; Reynaud, A.; Pojer, F.; Dilek, N.; Reichenbach, P.; Ascencio, K.; Irving, M.; Coukos, G.; Vogel, P. Azole-based indoleamine 2,3-dioxygenase 1 (IDO1) inhibitors. *J. Med. Chem.* **2021**, *64* (4), 2205–2227.

(60) Bedia, C.; Camacho, L.; Abad, J. L.; Fabrias, G.; Levade, T. A simple fluorogenic method for determination of acid ceramidase

activity and diagnosis of Farber disease. *J. Lipid Res.* **2010**, *51* (12), 3542–3547.